ANKARA YILDIRIM BEYAZIT UNIVERSITY

GRADUATE SCHOOL OF NATURAL AND APPLIED SCIENCES



THE EFFECT OF RADIATION ON THE CURRENT-VOLTAGE (I-V) CHARACTERISTICS OF $Au/Bi_4Ti_3O_{12}/SiO_2/n\text{-}Si$ (MFIS) STRUCTURES

M.Sc. Thesis by

Sezgin DULKADİR

Department of Electrical and Electronics Engineering

July, 2020

ANKARA

THE EFFECT OF RADIATION ON THE CURRENT-VOLTAGE (I-V) CHARACTERISTICS OF $Au/Bi_4Ti_3O_{12}/SiO_2/n\text{-}Si$ (MFIS) STRUCTURES

A Thesis Submitted to

The Graduate School of Natural and Applied Sciences of

Ankara Yıldırım Beyazıt University

In Partial Fulfillment of the Requirements for the Degree of Master of Science in Electrical and Electronics Engineering, Department of Electrical and Electronics Engineering

by

Sezgin DULKADİR

July, 2020

ANKARA

M.Sc. THESIS EXAMINATION RESULT FORM

We have read the thesis entitled **"THE EFFECT OF RADIATION ON THE CURRENT-VOLTAGE (I-V) CHARACTERISTICS OF Au/$Bi_4Ti_3O_{12}$/SiO_2/n-Si (MFIS) STRUCTURES"** completed by **SEZGİN DULKADİR** under the supervision of **ASSOC. PROF. DR. ÖMER KARAL** and we certify that in our opinion it is fully adequate, in scope and in quality, as a thesis for the degree of Master of Science.

Assoc. Prof. Dr. Ömer KARAL

Supervisor

Prof. Dr. Abdullah YILDIZ

Jury Member

Prof. Dr. Habibe TECİMER

Jury Member

Prof. Dr. Ergün ERASLAN

Director

Graduate School of Natural and Applied Sciences

ETHICAL DECLARATION

I hereby declare that, in this thesis which has been prepared in accordance with the Thesis Writing Manual of Graduate School of Natural and Applied Sciences,

- All data, information and documents are obtained in the framework of academic and ethical rules,
- All information, documents and assessments are presented in accordance with scientific ethics and morals,
- All the materials that have been utilized are fully cited and referenced,
- No change has been made on the utilized materials,
- All the works presented are original,

and in any contrary case of above statements, I accept to renounce all my legal rights.

Date: **Signature:**

Name & Surname: Sezgin DULKADİR

ACKNOWLEDGMENTS

I would like to express my best regards and my sincere gratitude to my thesis supervisor Assoc. Prof. Dr. Ömer KARAL who provides guide and support to me with his knowledge, experience, and encouragement.

I would like to express my sincere gratitude to Prof. Dr. Habibe TECİMER for his supervision, special guidance, suggestions, and encouragement through the development of this thesis.

I would like also to thank Ahmet KAYMAZ and Esra E. BAYDİLLİ for supporting my thesis study.

I would like also to thank Prof. Dr. Şemsettin ALTINDAL for supporting my thesis study.

I would like to thank my father Atila DULKADİR and my mother Döndü DULKADİR. In addition, I wish to thank my brother Sadullah DULKADİR and my sister Meltem DULKADİR who have been with me in every period of my life and who have supported me.

Date: 2020, July **Signature:**

Name & Surname: Sezgin DULKADİR

THE EFFECT OF RADIATION ON THE CURRENT-VOLTAGE (I-V) CHARACTERISTICS OF $Au/Bi_4Ti_3O_{12}/SiO_2/n$-Si (MFIS) STRUCTURES

ABSTRACT

Determining the radiation effects on the basic electrical parameters of the fabricated high-dielectric MFIS structures, they were exposure to the high-energic of ^{60}Co γ-rays. For this purpose, the values of ideality factor (n), zero-bias barrier height (Φ_{Bo}) and series resistance (R_s) of them were extracted from the forward biases I-V data before and after irradiation by using various method such as standard thermionic-emission (TE) theory, Cheung's and Norde functions. Additionally, the energy dependent profile of surface states N_{ss} were extracted by considering voltage dependent of n, Φ_{Bo}, and R_s and compared each other. Experimental results show that the reverse saturation current (I_o), n, and R_s values increase with increasing radiation dose, Φ_{Bo} decreases. When the value of R_s by considering in the calculation of N_{ss}, they were found considerably decrease. The observed low discrepancies between N_{ss} after irradiation show that the used a high-dielectric ferroelectric interlayer leads to an increase the resistance of MS across to radiation. This is more important to fabricated radiation-resisted an electronic device, especially in the satellites due to hard-radiation in space. As a result, N_{ss}, R_s and the existence of interlayer are more effectual on the I-V characteristics which must be considering in the electrical parameters calculation.

Keywords: $Au/(Bi_4Ti_3O_{12}/SiO_2)/n$-Si (MFIS) structures; Effects of gamma-radiation and series resistance; Energy dependent profile of surface states; Cheung and Norde Functions

RADYASYONUN $Au/Bi_4Ti_3O_{12}$ / SiO_2/ n-Si (MFIS) YAPILARININ AKIM-GERİLİM (I-V) ÖZELLİKLERİ ÜZERİNE ETKİSİ

ÖZ

Üretilen yüksek dielektrikli MFIS yapılarının temel elektriksel parametreleri üzerindeki radyasyon etkilerini belirlemek için, hazırlanan yapı ^{60}Co γ ışınlarının yüksek enerjisine maruz bırakıldı. Bu amaçla, standart termiyonik emisyon teorisi (TE), Cheung ve Norde fonksiyonları gibi çeşitli yöntemler kullanılarak radyasyondan önce ve sonra ileri voltaj I-V verilerinden idealite faktörü (n), sıfır-beslem potansiyel engel yüksekliği (Φ_{Bo}) ve seri direnç değerleri (R_s) hesaplanmıştır. Ek olarak, ara durumlarının N_{ss} 'in enerjiye bağlı profili, voltaja bağlı n, Φ_{Bo} ve R_s değerleri dikkate alınarak elde edildi. Deneysel sonuçlar, artan radyasyon dozu ile ters doyma akımı (I_o), n ve R_s değerlerinin arttığını, Φ_{Bo} değerinin azaldığını göstermektedir. N_{ss} hesaplamasında R_s değeri dikkate alındığında, önemli ölçüde azaldığı bulunmuştur. Radyasyon sonrası N_{ss} arasında gözlenen düşük tutarsızlıklar, kullanılan yüksek dielektrikli ferroelektrik ara katmanın, MS'nin radyasyona karşı direncinde bir artışa yol açtığını göstermektedir. Bu, özellikle uzayda sert radyasyon nedeniyle uydulardaki radyasyona dirençli bir elektronik cihaz için daha önemlidir. Sonuç olarak, N_{ss}, R_s ve ara katmanın varlığı, elektriksel parametrelerin hesaplanmasında dikkate alınması gereken I-V özellikleri üzerinde daha etkilidir.

Anahtar Kelimeler: $Au/(Bi_4Ti_3O_{12}/Si0_2)$/n-Si (MFIS) yapıları; Gama radyasyonunun ve seri direncin etkileri; Yüzey durumlarının enerjiye bağlı profili; Cheung ve Norde Fonksiyonları

CONTENTS

M.Sc. THESIS EXAMINATION RESULT FORM ii
ETHICAL DECLARATION iii
ACKNOWLEDGMENTS iv
ABSTRACT v
ÖZ.. vi
CONTENTS vii
NOMENCLATURE ix
LIST OF TABLES xi
LIST OF FIGURES xii
CHAPTER 1 - INTRODUCTION 1
1.1. Literature Review 1
1.2. Aim of Thesis 4
1.3. Thesis Overview 5
CHAPTER 2 - THEORY OF METAL-FERROELECTRIC-INSULATING SEMICONDUCTOR (MFIS) STRUCTURES AND GENERAL DEFINITIONS……..… 6
2.1. Definitions 6
2.1.1. Metals / Conductors 6
2.1.2. Ferroelectric Materials and Their Properties 7
2.1.3. Conductor, Insulator and Semiconductor Concepts 11
2.2. Basic Properties of Silicon Crystal 14
2.3. MIS and MFIS Structures 15
2.3.1. MIS Structure 16
2.3.2. Real MIS Structure 22
2.3.3. MFIS Structure 24
CHAPTER 3 - EXPERIMENTAL METHOD 28
3.1. Experimental Preparation 28
3.1.1. Creation of MFIS Structure 28
3.2. Experimental Measurement System 30
3.2.1. Keithley 2400 Current-Voltage Source 31
3.2.2. Janis vpf-475 cryostat 31
CHAPTER 4 - RESULTS and DISCUSSION 33
CHAPTER 5 - CONCLUSION 45

FUTURE WORK……47
REFERENCES..... 48
CURRICULUM VITAE..... 54

NOMENCLATURE

Symbols

V	Applied voltage
χ	Electron susceptibility of the semiconductor
k	Boltzmann constant
K	Temperature in Kelvin
E	Electric field intensity
C	Capacitance
I	Current
Å	Angstrom
Q	Electric charge
C_{OX}	Interfacial layer capacitance
A^*	Effective Richardson constant
d_{ox}	Oxide thickness
ψ_s	Band tension on the interface
χ_s	Electron affinity of semiconductor
ψ_s	Surface potential
ε_0	Dielectric constant of space
ε_s	Dielectric constant of semiconductor
ε_{ox}	Dielectric constant of the oxide layer
C_{SS}	Interface capacitance
W_D	Depletion area thickness
Q_{SC}	Space charge in the semiconductor
R_S	Series resistance
R_i	Resistance value

N_{ss}	Interface state density
Φ_B	Potential barrier height
Φ_{BO}	Zero bias barrier height
ω	Angular frequency ($2\pi f$)

Acronyms

MS	Metal-Semiconductor
MIS	Metal-Insulator-Semiconductor
MOS	Metal-Oxide-Semiconductor
MFIS	Metal-Ferroelectric-Insulator-Semiconductor
MFM	Metal-Ferroelectric-Metal
FET	Field Effect Transistor
FeRAM	Ferroelectric Random Transition Memory
FeFET	Ferroelectric-Based Field Effect Transistor
BTO	$Bi_4Ti_3O_{12}$
BLSF	Bismuth-Layered-Structure Ferroelectric
RFID	Radio Frequency Identification
I-V	Current-Voltage
HF	High Frequency
LF	Low Frequency
Al	Aluminum
Au	Gold
Si	Silicium

LIST OF TABLES

Table 4.1. The basic electrical parameters of the structure. 35

Table 4.2. Basic electrical parameters of the structure obtained from Cheung Functions. 40

Table 4.3. Basic electrical parameters of the structure obtained from Norde Functions. ..…….....42

LIST OF FIGURES

Figure 2.1 Illustration of a layered perovskite ferroelectric structure containing bismuth: 8

Figure 2.2 Electromagnetic radiation spectrum……..10

Figure 2.3 Atomic representation of conductor, insulator and semiconductor 12

Figure 2.4 Energy band diagrams for insulating, semiconductor, conductive material 12

Figure 2.5 Crystal structure of silicon atoms and a simple cubic crystal structure... 15

Figure 2.6 Schematic representation of an MIS structure 17

Figure 2.7 Energy-band diagrams of ideal MIS capacitors at equilibrium (V=0). (a) n-type semiconductor. (b) p-type semiconductor. 18

Figure 2.8 Equivalent circuit of a MIS structure 20

Figure 2.9 Energy band diagram of the ideal MIS structure at V≠0 (a) Accumulation (b) Depletion (c) Inversion 21

Figure 2.10 Electronic scheme of an ideal MIS structure in (a) Accumulation, (b) Depletion and (c) Inversion states 22

Figure 2.11 Interface states and classification of charges for a non-ideal MIS / MOS structure 23

Figure 2.12 Schematic representation of the metal-ferroelectric-insulator-semiconductor structure 25

Figure 2.13 Energy band diagrams for different work zones for an MFIS structure 26

Figure 3.1. The schematic view of the copper masks used when forming the (a) top and (b) bottom contacts of the structure 29

Figure 3.2 Vacuum device which used to create ohmic and rectifier contacts 29

Figure 3.3 The cross-sectional areas of the created MFIS structure are shown schematically. 30

Figure 3.4 Keithley 2400 current-voltage source 31

Figure 3.5 Janis vpf-475 cryostat 32

Figure 4.1 I-V graphs of the structure. 34

Figure 4.2 Ri characteristics of the structure. 37

Figure 4.3 dV/d(LnI)/H(I)-I plots of the structure for before. 39

Figure 4.4 dV/d(LnI)/H(I)-I plots of the structure for 5 kGy. 39

Figure 4.5 dV/d(LnI)/H(I)-I plots of the structure for 22 kGy. 40

Figure 4.6 F(V)-V plots of the structure. 42

Figure 4.7 The density of Nss profiles as a function of (Ec-Ess). 44

CHAPTER 1

INTRODUCTION

Technology is everything that human beings do to make human life easier by using science. Technology is of great importance in human life. For this reason, the importance of various materials that we will use in the development of technology and the elements created from these materials are increasing for us day by day. Especially one of the most important works of today is for various microelectronic and optoelectronic devices in computer and fiber optic telecommunication systems; It relates to semiconductors and ferroelectrics, which are very important components of applications such as computing, memory storage and communication.

1.1. Literature Review

According to recent researches, ferroelectric materials with various physical properties have been used in important studies [1-3]. Ferroelectric thin films have an important place in many technological applications such as ferroelectric memories and piezoelectric devices. Ferroelectric thin films, positioned to form sandwich structures between metal electrodes, have been subject to considerable research and have been developed as memory media in ferroelectric random access memories (FERAM). FERAMs are stable memories and have the ability to store information without a power source. It has long been known that ferroelectric systems operate with a metallic electrode and for device physics, metal ferroelectric interfaces have been an important research topic. Due to these properties of ferroelectric materials, FERAMs have been developed as memory media.

Permanent and stable solid-state memories have an important place in information technologies. When compared with magnetic and optical mass storage devices, it can be said that they are stronger and have faster data entry time. This is because they have no moving parts. FERAMs are of considerable importance for low power and very low voltage applications such as battery-powered embedded systems, smart cards and radio frequency identification (RFID) application [4].

Due to its effective usage areas and important characteristics in recent years, FERAM has an important place in today's technology. Among them are outstanding speed performance, high information density, unlimited read-write cycles, wide operating temperature range and the ability to serve in a harsh environment that serves as part of portable IC cards or even radiation-resistant aerospace equipment [6]. Field effect transistor (FET) memories are a source of inspiration for today's work. FETs are preferred in many areas because they work extremely sensitive and fast responsive [7]. Ferroelectric field effect transistors (FeFET) are an example of fixed memories. FeFET memory is of great importance in comparison with its alternatives due to non-destructive reading, low power consumption, fast read / write and flash-like structure mark features [8]. Because FETs can develop with today's technology, its importance has gained a worldwide dimension. The FeFET is a Metal Oxide Semiconductor FET (MOSFET) containing a ferroelectric layer, which is placed between the silicon surface and the gate electrode also there are many studies about FeFET in the past that inspired today's work [9].

Although FeFET's work has been done for years, it is still difficult to find the ideal device. Among the identified problems, the most remarkable is the lack of memory time. Constructive solutions such as achieving low interface state density, developing production technology for gate stacking, and using new materials are among the current studies.

Bismuth titanate (BTO) is known as a good ferroelectric material due to its high Curie temperature (675 °C), high piezoelectric coefficient and strong anisotropic spontaneous polarization from BLSF (bismuth-layered-structure ferroelectric) [5]. Due to this characteristic of BTO, it finds wide application in high temperature piezoelectric devices and memory storage devices. $Bi_4Ti_3O_{12}$ is a member of which Aurivillius-phase ferroelectrics (bismuth layer-structured ferroelectrics, BLSFs) with the general formula of $(Bi_2O_2)^{2+}(A_{n-1}B_nO_{3n+1})^{2-}$ [10]. Owing to Bismuth titanate's useful properties, for example; low coercive field and peculiar switching behavior, fatigue endurance, high dielectric permittivity, fatigue resistance as well as from BLSF with high Curie temperature (675 °C), high piezoelectric coefficient and strong anisotropic spontaneous polarization, diverse forms of bismuth titanate have become

materials of attractive for diverse implementations such as nonvolatile random-access memories (NVRAMs), ferroelectric random access memories and ferroelectric field effect transistor [3, 9] . BTO is also very effective in the development of ferroelectric random access memory and array antennas. BTO at room temperature has a pseudoorthorombic structure with a = 5.41 Å, b = 5.45 Å and c = 32.83 Å weave constants. Unit cell that forms 2 units of the BTO formula length is 32 Å. In addition, in recent years, since lead-free materials are environmentally friendly, research has focused on lead-free ferroelectric materials. Bismuth titanate is a well-known lead-free bismuth layered structure ferroelectric with high Curie temperature (675 °C) [12].

Ferroelectric materials have a hysteresis curve because such materials have polarity-electric field interaction. If we want to get information about the memory window of the ferroelectric material, we can benefit from the hysteresis curve. Although there are many structures to investigate ferroelectric behavior, capacitors are the simplest. Ferroelectric (BTO) thin films were placed between metal electrodes to form a sandwich structure, studies were made and FeRAMs were created [3,11]. Metal ferroelectric metal (MFM) structure consists of metal or conductive metal oxide on the ferroelectric material. Metal ferroelectric semiconductor (MFS) structures, a kind of metal-oxide-semiconductor structure, are the most remarkable structures in semiconductor technology. Due to the structural imperfection in creating this structure, the desired structure has been converted to MFIS structure. MFS structure was converted to MFIS structure using a thin insulating layer such as SiO_2, SnO_2 and Si_3N_4 at BTO / Si interfaces. This superior thin surface insulating layer (SiO_2) prevents the reduction of the electric field as it regulates charge transitions in the MFIS structures. It also prevents internal diffusion between ferroelectric film (BTO) and Silicon (Si) [14]. MFIS ferroelectric layer provides memory capability to MOS capacitor[15]. In addition to the experiments carried out during the production stage, several theoretical models have been prepared to describe the properties of MFIS structures. As a result of these theoretical models, it was found that MFS is easy to produce and has non-destructive reading capability. MFIS structures, gate leak doesn't influence the stabilization of the ferroelectric, and internal MOSFET gate oxide and the ferroelectric material may every time be properly chosen so as to ensure the stability of the negative capacitance effect in steady state [16]. In MFIS structures, capacitive features are

added to these devices in the presence of an interface insulating layer. Due to the dielectric property of the insulating layer, the electrical charge is shared. This event affects the basic electrical parameters of the structure. In an MFIS structure, the metal and the semiconductor are separated by an insulating layer and the distribution of surface states at the semiconductor / insulator interface is continuous. If a voltage is applied to the MFIS structure, the interface insulating layer, the consumption layer and the series resistor divide this voltage within themselves.

The quality and performance of metal-insulating semiconductor or metal-oxide-semiconductor, metal-ferroelectric-semiconductor and metal-ferroelectric-insulating semiconductor structures rely on a lot of factors such as the existence of interlayer, its thickness, the preparation of surface, the concentration of doping atoms, series resistance (R_s) and surface/interface states (N_{ss}) of the sample, measurement conditions such as temperature, frequency and applied electric field. Among these factors, the interfacial layer, N_{ss} and R_s have considerable effects on several other electrical. Although many methods have been developed for the determination of R_s, it was obtained by three different methods: Ohm's Law, Cheung and Norde methods. Energy distribution profile of N_{ss} as a function of ($E_c - E_{ss}$) was obtained from the forward bias I-V characteristics.

1.2. Aim of Thesis

In recent years, techniques applied in surface and interface science reveal that interfaces formed between metal and semiconductors are complex regions. The physical properties of these complex areas depend on the preparation conditions of the surface. In many cases, metal contacts cause interface conditions on surfaces with unknown contents. These interface states can affect the stability, accuracy, performance, electrical and mechanical properties of metal-semiconductor structures. In a MIS structure, interface states are much less when compared to that of the metal-semiconductor (MS) structure. Because, when voltage is applied to the MIS structure, the interface insulating layer, consumption layer and series resistance share this applied voltage. In the light of the information obtained, the studies are concentrated on MIS structures. Then, by placing a ferroelectric material between the metal and

insulating layer, it was thought that metal-ferrolectric-insulator-semiconductor structures would be created, in this way some surface problems could be solved and studies in this field have come to the agenda [17].

Today, current voltage characteristics of MS, MIS, MOS or MFIS structures are investigated taking into account the interfacial state density (N_{ss}), series resistance (R_s) and insulating layer effect depending on the radiation effect [16,17]. The main purpose of these studies is to develop stable memory devices based on MFIS. These non-destructive readout structures are used both as non-volatile storage capability and sensitivity elements [20]. MFIS structures are formed by the addition of a thin insulating layer between the ferroelectric material and the semiconductor layers using a natural or artificial oxidation method [21]. In addition to regulating the charge transition, this insulating layer insulates the metal and the semiconductor from each other.

1.3 Thesis Overview

In Chapter 1 of this study, the technological development of ferroelectric memory elements is mentioned. In Chapter 2, general information about the properties of the materials used to create the structure and other similarly formed structures are given. In Chapter 3, information is given about the, preparation stages of Au/($Bi_4Ti_3O_{12}$/SiO_2)/n-Si (MFIS) structures, experimental measurement systems, and measuring devices used. In Chapter 4, all the graphs and charts of the experimental results obtained are given. In Chapter 5, the results obtained before and after the radiation effect applied to the structure are expressed.

CHAPTER 2

THEORY OF METAL-FERROELECTRIC-INSULATING SEMICONDUCTOR (MFIS) STRUCTURES AND GENERAL DEFINITIONS

In this section, the theory of MFIS structures and some specific definitions are mentioned. The basic physical properties of the insulating layer grown between the ferroelectric material (BTO) and the semiconductor layer (n-Si) are also described. The insulating interface layer (SiO_2) that we use in our study is formed by methods such as natural or thermal oxidation between the ferroelectric material and the semiconductor. We can give examples of insulating interface layer such as SiO_2, SnO_2 and Si_3N_4. To better understand MFIS structures, we need to draw more attention to the basic concepts that make up these structures. Therefore, it is necessary to mention briefly the concepts of metal, ferroelectric, insulator and semiconductor.

2.1. Definitions

2.1.1. Metals / Conductors

Metals commonly found in nature are elements that stand out with their high electrical and thermal conductivity [22]. There are many reasons for the widespread use of metals in nature, for example, they can be formed into the desired shape and interact with other metals to obtain a desired element.

In semiconductor devices and MS, MIS, MFIS structures, very pure metals are used to form ohmic and rectifier contacts and suitable metals such as Al and Au are selected according to the type of semiconductor (type n or type p) [23]. In this study, while rectifying MFIS structure, rectifier and ohmic contacts were obtained by using pure gold (99.999%).

2.1.2. Ferroelectric Materials and Their Properties

One of the main characteristics of ferroelectric materials is that it has a high dielectric constant and its dielectric properties depend on temperature and electric field [24]. On the other hand, ferroelectric materials have both piezoelectric and pyroelectric properties.

Ferroelectric materials have become a promising material in non-volatile memory storage devices and nonlinear optics. Furthermore, ferroelectric materials can be used in the production of capacitors for the electronics industry due to their high dielectric constant and have a new perspective in terms of the multifunctional and miniaturization of electronic products. In addition, ferroelectric materials are used in the construction of microwave devices used in the fields of satellites, earth communications and other microwave applications.

Three of the most important features to be considered in the characterization of ferroelectric materials are as follows; firstly, the dielectric constants of these materials are quite high, secondly, the application forms of the dc electric field and finally, the third is how to control the measurement temperature.

The first experiments on ferroelectric memory were conducted by Moll and Tarui in 1963 at Stanford University [25]. The basic idea for this device is that there is memory function in a ferroelectric material and that it can control the field-effect transmission of a semiconductor by residual polarization in the ferroelectric material. At the time of the study, the experience with semiconductors was greater than that of ferroelectric thin films, and therefore the combination of single crystal ferroelectric material with semiconductor was preferred [25].

In recent years, ferroelectric memory devices have become very interesting in terms of usability in new generation complex circuits in various applications. Extensive studies have been carried out on the formation of ferroelectric thin films into metal electrodes in sandwich structures and they have emerged as FeRAMs.

FeRAMs are capable of storing information without the use of a power source, and also have inherent superior speed performance, high information density, unlimited

write-read cycles, wide operating temperature range [4,5]. To better understand FeRAMs, a metal ferroelectric-metal (MFM) type capacitor has been studied [60].

Another ferroelectric memory element is FeFET. Ferroelectric field effect transistors and field effect transistors use ferroelectric thin films to form metal-ferroelectric-semiconductor structures. FeRAM is a typical ferroelectric material which is a candidate for use in optical memory and imaging, electro-optical devices, high temperature piezoelectric structure and permanent memory.

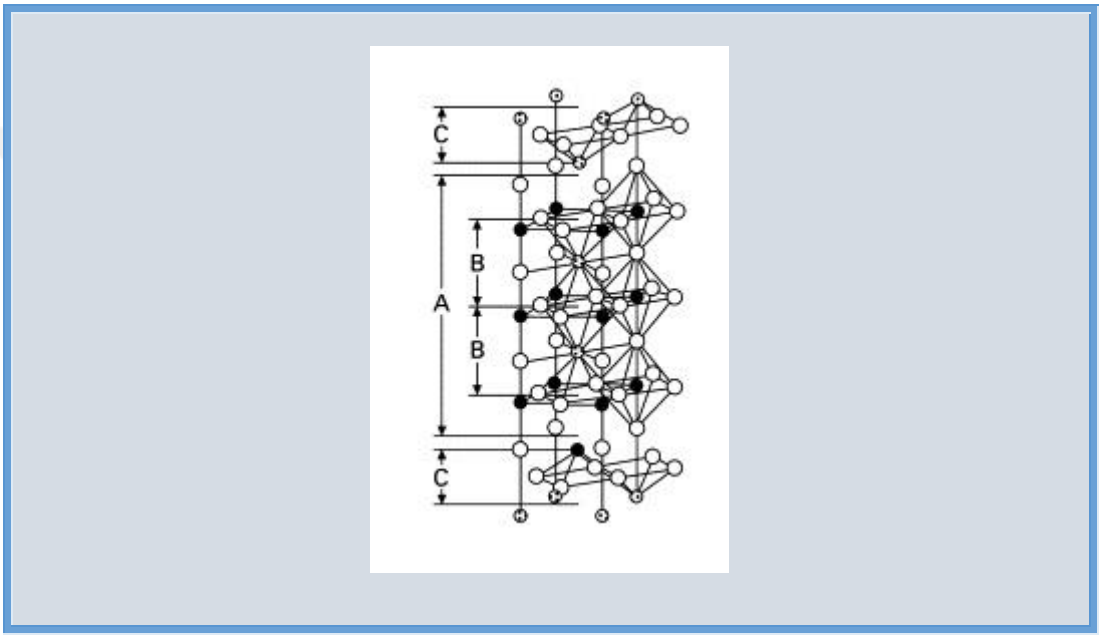

Figure 2.1. Illustration of a layered perovskite ferroelectric structure containing bismuth:
A- perovskite layer, B- unit cell, C- bismuth oxide layer

Figure 2.1 shows a schematic representation of a layered perovskite ferroelectric structure containing bismuth. Bismuth titanate $Bi_4Ti_3O_{12}$, has attracted significant interest in the applications of devices such as nonvolatile FeRAMs, optical memory, piezoelectric, and electro-optic devices due to its low coercive field, high Curie temperature (675 °C), high dielectric constant, high breakdown strength and peculiar switching behavior [9–11]. As a result of research, BTO can reduce the magnitude of leakage current N_{ss}, R_s and it can increase rectifier rate also it is interesting because of

its unique electro-optical on-off behavior [26]. In this study, $Bi_4Ti_3O_{12}$ thin film was used as ferroelectric material.

Radiation Dependence of Ferroelectric Materials

Radiation is a type of energy that radiates from unstable atoms that have undergone radioactive decay, in the form of energy waves or energetic particles. Considering this definition, we can understand that there are two different types of radiation: electromagnetic wave type radiation and particle type radiation. In addition to the propagation of electromagnetic radiation in the form of electric and magnetic waves without mass, it can also be in the form of ionizing or non-ionizing radiation, depending on the magnitude of the energy. Particle-type radiation is a type of radiation that has mass and a large amount of energy. Therefore, it is possible to say that such radiation is also ionizing radiation. Non-ionizing radiation has enough energy to move atoms in a molecule or cause them to vibrate, but not enough energy to remove electrons from atoms. Radio waves, visible light and microwaves are examples of this type of radiation. Ionizing radiation, on the other hand, has enough energy to remove the electrons from atoms, that is, to carry out the ionization process. Since ionizing radiation can also affect atoms in living things, it can create a health risk by damaging the tissues and DNA in the genes. X-rays emitted from devices, cosmic particles and radioactive elements from space are examples of ionizing radiation.

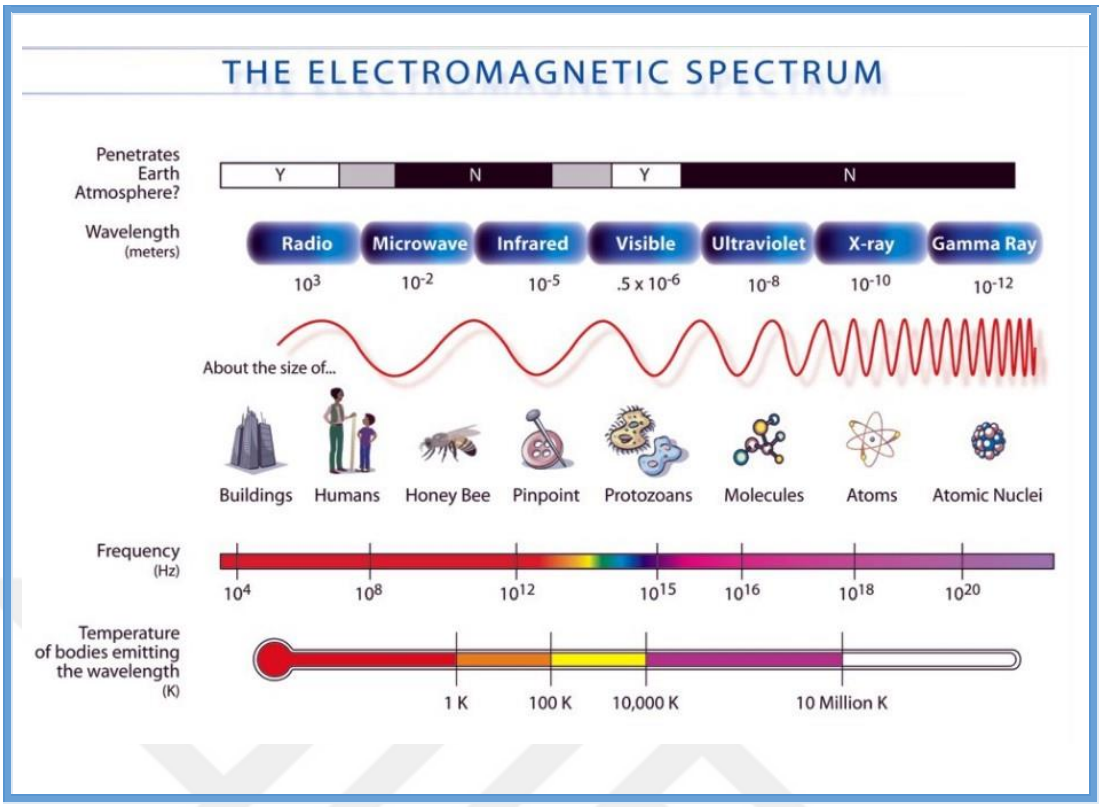

Figure 2.2. Electromagnetic radiation spectrum

The wavelengths and energies of gamma rays are very high, which shows that these rays are in the ionizing radiation group. Gamma rays can easily pass through layers like wood, paper and fine aluminum. Therefore, the effect areas of this type of rays are quite wide. Gamma rays may exist in biomedical and industrial applications as well as in space applications. Therefore, it is important to understand the electrical characteristics of the electronic device components to be used in these applications according to the dose of gamma rays. On the other hand, the production of materials whose electrical characteristics are not impaired under the influence of gamma-rays will also increase the reliability of applications in these areas.

It is known that radiation has two important effects on materials, generally permanent and temporary [27]. While the formation of recombination of electron-hall pairs from these effects is seen as a temporary effect, the crystal structure defect/change in the materials due to radiation bombardment is considered as a permanent effect. The research of these two important effects on the MFIS structures used in our study has been examined in detail.

The presence of an interfacial insulator layer in MFIS structures makes them rather sensitive to radiation. Radiation damage is usually found at or near the Si/SiO_2 interface. In the light of the information given above; extensive studies have been carried out for many years and it has been discovered that radiation has significant effects on MFIS structures, such as positive charge accumulation in oxide and the formation of new electron states at the Si / SiO_2 interface [28]. Ionizing radiation damages to the MFIS structures both by creating positive charges in the oxide layer and by trapping negative charges at the interfaces of the MFIS structures. Winokur et al. [29] and Ma [30] were among the first to make a systematic observation of the after irradiation behavior of radiation-induced interface traps in MFIS structures. The transient effects due to the electron–hole pair generation and permanent effect due to the bombardment of devices with radiation, which are cause changes in the crystal lattice, are significant effects of radiation to be considered. The radiation-generated holes that are less mobile than electrons can spread in insulators, furthermore, there are many stationary hole traps.

2.1.3. Conductor, Insulator and Semiconductor Concepts

The transfer of electric energy as a result of vibration motion of negative charges is called electric current. The movement of electrons in each material is not the same, that's why, according to the movement of electrons, the materials are divided into three categories conductors, insulators and semiconductors. Figure 2.2 shows the atomic representation of these materials.

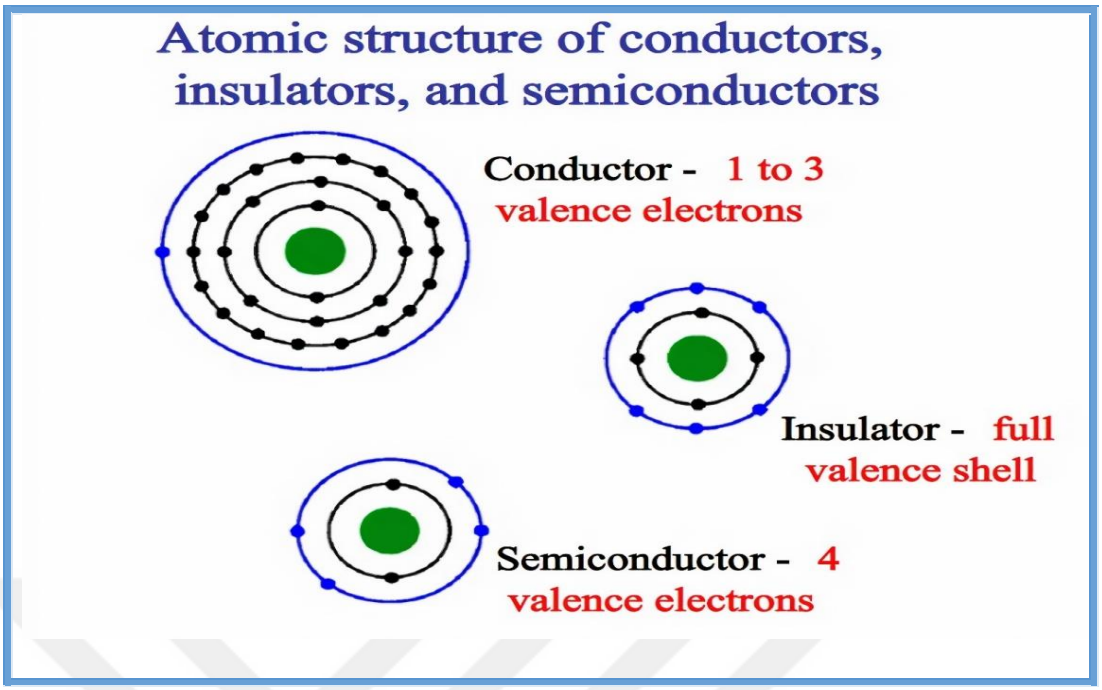

Figure 2.3. Atomic representation of conductor, insulator and semiconductor

Energy band diagrams of insulating, semiconductor and conductive materials are given in Figure 2.4

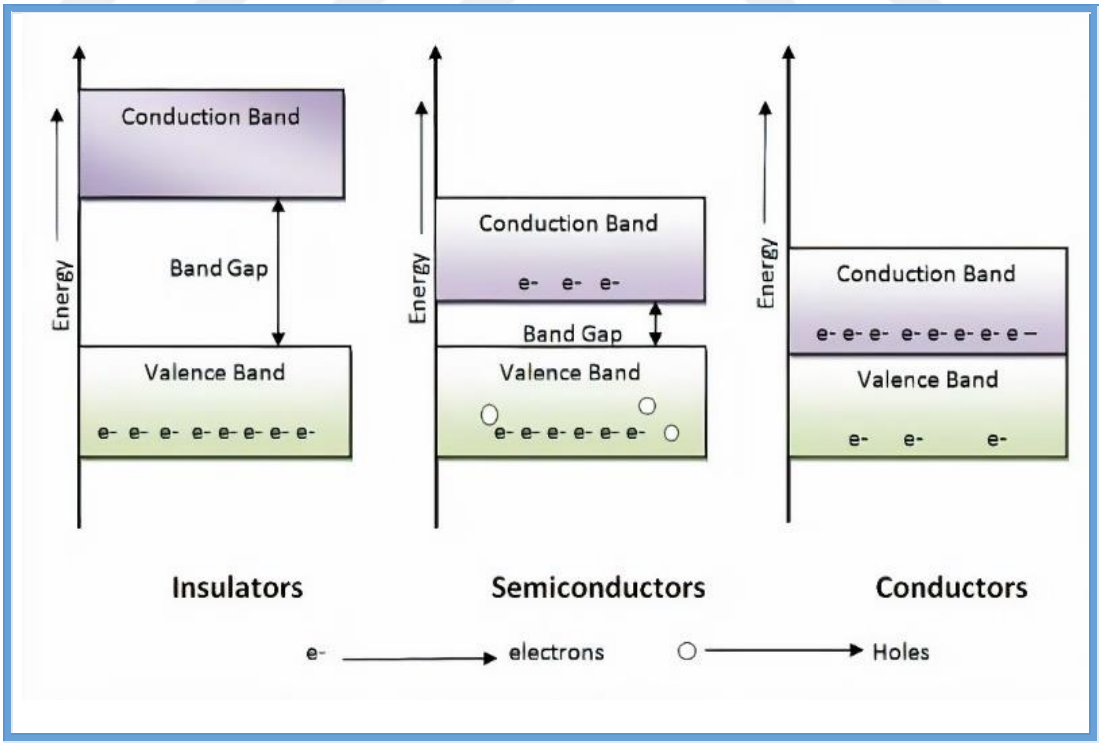

Figure 2.4. Energy band diagrams for insulating, semiconductor, conductive material

Properties of conductors

*They conduct electrical current well and have high conductivity.

*The electrons in the outer orbit of atoms are weakly attached to the atom. They are easily separated from the atom under heat, light and electrical effects.

*Valence band and conductivity band are intertwined.

*Heat or electrical conductivity of conductors is between 10^4-10^6 Ω/cm and decreases with increasing temperature.

Properties of insulators

*Non-conductive materials are called insulators.

*The electrons in the last orbit of the insulators are tightly attached to the atom

*Insulators have very high resistivity

*The forbidden energy range is very wide for insulators ($E_g \geq 4$ eV)

Properties of semiconductors

*They are among conductors and insulators in terms of conductivity.

*They are normally insulated.

*When it is exposed to heat, light and magnetic effect or voltage is applied, some valence electrons are released, that is, they become conductive.

*They are found as simple elements in nature and they are also obtained as compound elements in the laboratory.

*The coefficient of variation of resistance with temperature is generally negative.

Germanium and silicon are semiconductors used in electronics and are widely used in diodes, transistors and integrated circuits. The most important distinguishing feature of a semiconductor is that its conductivity depends on temperature. In other words, in

semiconductors, conductivity increases with increasing temperature, and in metals, conductivity decreases with increasing temperature. For a semiconductor there are many parameters in determining the range of applications, the most important of which is the forbidden energy range. In other words, it is the energy separation between valence and energy bands and is in the range of 0-4 eV for semiconductors. The silicon carries 4 electrons in the outer orbit. If a Si atom in a silicon crystal is replaced by a substance that carries 5 electrons in the outer orbit, such as nitrogen or phosphorus, a covalent bond forms with four of the five outer shell electrons. The fifth electron remains attached to phosphorus with a very small energy (0.04 eV). As the phosphorus releases this electron, the number of electrons in the conduction band increases. N-type semiconductor occurs when the electron density in the semiconductor is greater than the hall density. Arsenic and antimony are also used for this purpose.

If boron or aluminum with 3 electrons in the final orbit is used, the substance formed is poor and receives electrons and the semiconductor formed in this way is called p type semiconductor. Here electron carriers are positive. Here electron carriers are positive. Indium is also among the substances used for this type of study. A wide variety of semiconductor circuit elements can be made by bringing p and n type materials together side by side.

2.2. Basic Properties of Silicon Crystal

Silicon (Si), which is an insulator at low temperatures, is one million times more conductive at 20 ^{o}C than insulators, but its conductivity is 100 million times less than metals. The doping process occurs as a result of mixing the substances mentioned above with a small amount of 3 or 5 electrons in its final orbit. Due to these properties, silicon is mostly used in semiconductor electronic circuit elements. In Figure 2.5, the crystal structure of silicon atoms and a simple cubic crystal structure are shown schematically.

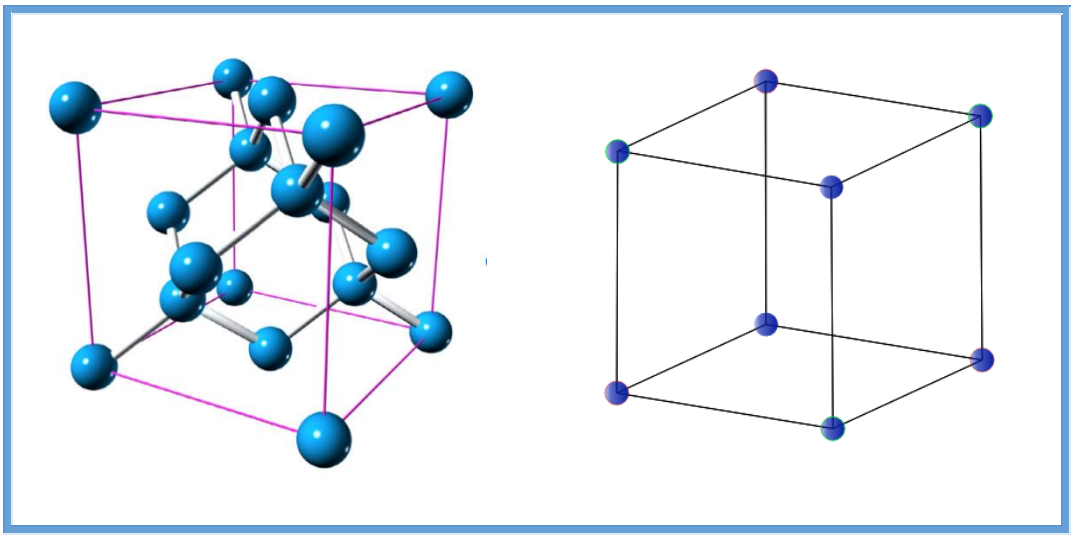

Figure 2.5. Crystal structure of silicon atoms and a simple cubic crystal structure

Many steps are followed to achieve pure silicon, and it is finally brought to chemical purity, but the silicon semiconductor that is brought to chemical purity is not yet pure enough for electronic element construction. For this reason, the physical purification method is used. In the method called regional melting, semiconductor is purified from unwanted impurities by making use of the fact that some impurities dissolve much faster in liquid semiconductors [31]. The semiconductor purified by this method is still polycrystalline. After that, the semiconductor is enlarged into a single crystal and impurity (additive) substances that will provide the desired resistivity must be doped. The type of doping impurity determines the type of semiconductor and its amount (n) helps us understand the conductivity or resistivity ($\rho = 1/\sigma = 1/\mu en$). Silicon (Si) is one of the most abundant elements on earth. In addition to the abundance of silicon in nature, it has increased the importance of easily obtaining a natural insulating layer such as SiO_2 on the crystal surface. Integrated circuits and computers rely on silicon technology due to its semiconductor feature and abundance in nature, as well as its practical use in transistors, diodes and memories. Silicon, as is known, is the most used semiconductor material in the electronics industry.

2.3. MIS and MFIS Structures

Metal-semiconductor (MS) contacts, the simplest structure, have an important place in modern electronics. When the metal is contacted with the semiconductor, charge

transitions (diffusion) occur between the metal and the semiconductor until the thermal equilibrium is established. Until the Fermi energy levels of metal and semiconductors are equal, there are charge transitions from both metal to semiconductor and from semiconductor to metal. Researches on metal-semiconductor contacts are increasing day by day, especially in terms of better understanding of the current-transmission mechanisms physics of these structures. Metal-semiconductor contacts form an important part of almost all semiconductor electronic and optoelectronic devices. In today's technology, studies on these structures are still ongoing. Studies on MIS structures formed with the addition of an insulating layer to the metal-semiconductor interface and studies on MFIS structures created with the addition of a ferroelectric-insulating layer still attract attention.

2.3.1. MIS Structure

Metal-insulator-semiconductor (MIS) structures are similar to capacitors because they have an insulating layer between metal and semiconductor. These structures were first introduced by J.L.Moll in 1959 [25]. MIS structures are widely used in the investigation of the electrical properties of insulating thin films and semiconductor surfaces. Terman used a thermally oxidized semiconductor silicon crystal and aluminum metal electrode on MIS structure[32].

Grove, Deal, Snow and Sah performed the first detailed representation of the I-V data of metal-oxide-semiconductor (MOS) capacitors used in transistors and the magnification of the oxide layer on semiconductor surfaces [33]. If the insulating layer thickness in MIS structures is greater than 100 Å, MIS structures are called MOS structures. When the insulating layer thickness is very thin (~ 10-40 Å), these structures are called the MIS type Schottky diode and their electrical parameters are obtained using experimental measurements such as radiation-dependent current-voltage (I-V). An MIS structure is given schematically in Figure 2.6.

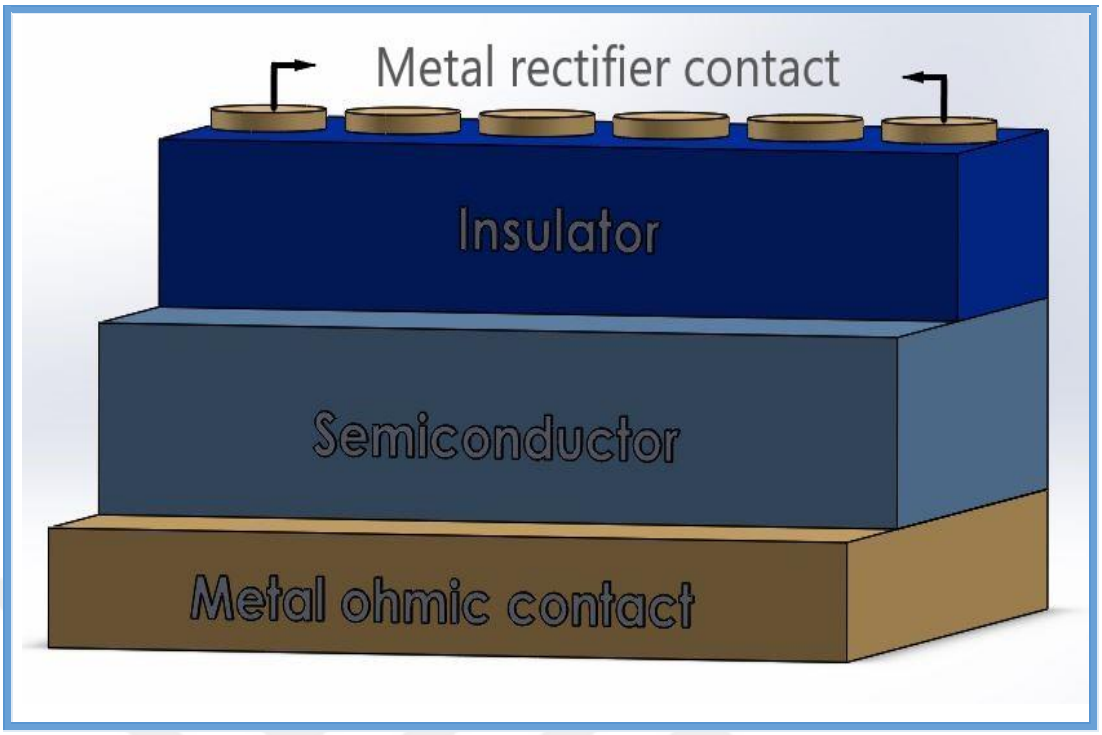

Figure 2.6. Schematic representation of an MIS structure

The prominent properties of these structures are determined by the properties of the insulator and insulator semiconductor interface. At the absolute zero temperature of conductors (T = 0 K), the difference between the ground state and the highest energy level is called *Fermi energy*. In semiconductors, *Fermi energy level* occurs at a level close to the conductivity or value band, depending on the additive status. *Vacuum level*: It is defined as the energy level of an electron with zero kinetic energy just outside a metal or the minimum amount of energy needed to remove an electron from the surface. *Work function of metal* (φ_m): It is defined as the minimum amount of energy needed to stimulate an electron from Fermi energy level to vacuum level. *Semiconductor work function* (φ_s), the energy difference between the Fermi energy level of the semiconductor and the vacuum level and this energy level is a varying quantity since it depends on the density and temperature of the additive atoms. *Electron affinity* (χ) is the energy difference of an electron between the vacuum level and the conduction band of the semiconductor. The schematic representation of the ideal MIS structure is given in Figure 2.7 for p-type and n-type semiconductors.

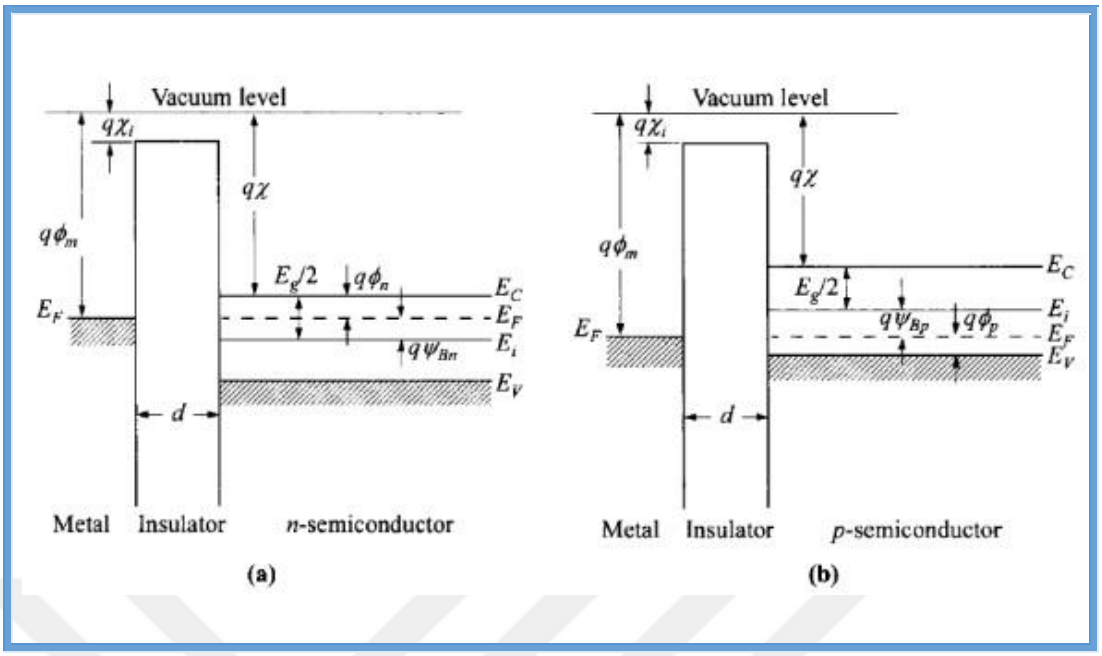

Fig 2.7 Energy-band diagrams of ideal MIS capacitors at equilibrium (V=0). (a) n-type semiconductor. (b) p-type semiconductor.

Here;

Φ_m : Work function of metal

Φ_B : Potential barrier height between metal and insulator

χ : Electron susceptibility of the semiconductor

χ_i : Electron susceptibility of the insulator

E_V : Valence (value) band energy level

E_C : Conductivity band energy level

E_i : Pure fermi energy level ((E_C-E_V)/2)

E_F : Fermi energy level

ψ_B : The difference between the fermi and the pure fermi energy level

$$\Phi_{\text{ms}} = \Phi_m - (\chi + \frac{E_g}{2q} - \psi_B) = 0 \qquad \text{(n-type)} \qquad \textbf{(2.1)}$$

$$\Phi_{ms} = \Phi_m - (\chi + \frac{E_g}{2q} + \psi_B) = 0 \qquad \text{(p-type)} \qquad \textbf{(2.2)}$$

E_g here; forbidden energy range of semiconductor and ψ_B is defined as the energy difference between the Fermi Energy level E_F and the initial energy level E_i. The insulating layer is an ideal dielectric material as the energy band gap is very large. In the insulating layer and insulator-semiconductor interface, traps, fixed and mobile ions, interface states and interface charges are not desired. The charge carrier density of the insulator in the transmission band is small enough to be neglected and the resistivity of the insulator is endless. The charges in the semiconductor are mostly and minority carriers according to the type of additive, and depending on the applied voltage, accumulation is observed. In an ideal MIS structure, when a voltage is applied to the rectifier contact, the charge shifts occur in the semiconductor. The density of free charges in the semiconductor depends on the applied voltage and is less than in the metal. In the semiconductor interface, space charges (Q_{sc}) are formed, which cause the band to bend. In the case of thermal equilibrium, the density of these charges is determined by the magnitude of the potential. The applied V_G voltage partially falls on the semiconductor / insulator interface. That's why,

$$V_G = V_{OX} + \psi_S \qquad \textbf{(2.3)}$$

equation can be written. Here, V_{ox} is the voltage falling on the insulating interface layer and ψ_S is the band voltage at the interface. The total charge in the system is determined by the following equation, considering the charges in a capacitor.

$$Q_m = Q_n + qN_AW = Q_S$$

$$Q_m + Q_{sc} = 0 \qquad \textbf{(2.4)}$$

Here, Q_n is the total charge of electrons per unit area in the inversion region and qN_AW is the number of ionized receiving additive atoms in unit area in space charge and space charge area and in the width of W. Q_s is the total charge in the semiconductor,

Q_m is the total charge on the metal surface and Q_{sc} is the charge accumulated in the space charge region [34]. The properties of the capacitors determine the insulating layer between the metal and the semiconductor and the insulator / semiconductor interface. Due to the insulating layer between the metal / semiconductor layer, a capacitance occurs between the metal and the semiconductor. The value of the capacitance depends on the dielectric constant of the interface. The equivalent circuit corresponding to an MIS capacitance is shown in Figure 2.7. If the applied voltage has small differential changes, the MIS structure can be shown as capacitance C, insulating layer capacitance C_{ox}, and space charge capacitance C_{sc}. Their equivalent capacitance will give us the MIS capacitance.

$$C = \frac{dQ_m}{dQ_G} A_{ox} \quad \textbf{(2.5a)}$$

$$C_{ox} = \frac{dQ_m}{dV_{ox}} A_{ox} \quad \textbf{(2.5b)}$$

$$C_{sc} = \frac{dQ_{sc}}{d\psi_s} A_{ox} \quad \textbf{(2.5c)}$$

Here, A_{ox} is the area of the insulating layer between the metal and the semiconductor, hence the MIS rectifier contact area.

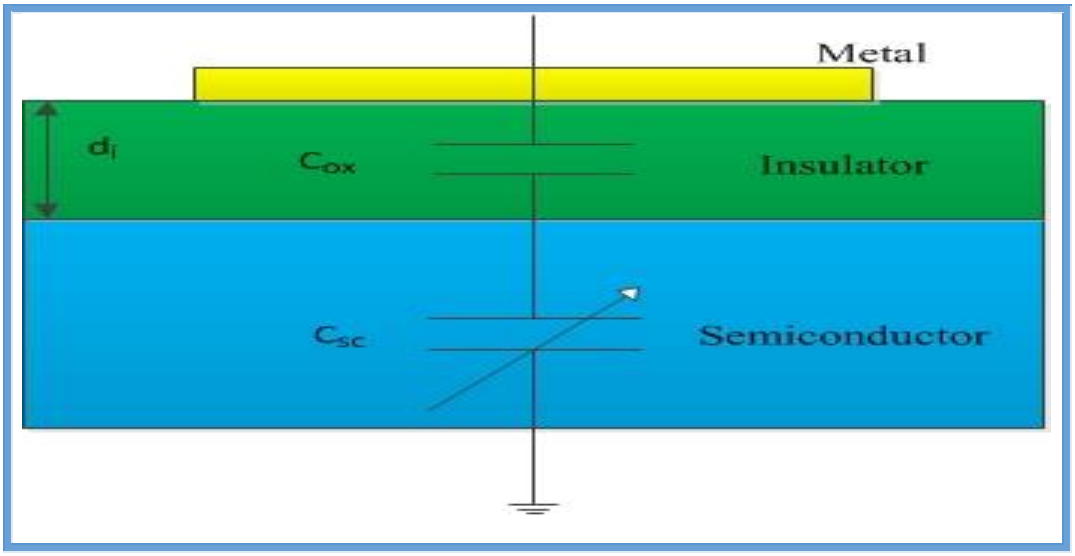

Figure 2.8. Equivalent circuit of a MIS structure

As seen in Figure 2.8, the equivalent capacitance of the MIS structure is equal to serial connection of C_{ox} (surface charge capacitance) and C_{sc} (insulating oxide capacitance).

$$\frac{1}{C} = \frac{1}{C_{sc}} + \frac{1}{C_{ox}} \tag{2.6}$$

Insulating oxide capacitance C_{ox} ,

$$C_{ox} = \frac{\varepsilon_{ox}}{d_{ox}} A_{ox} \tag{2.7}$$

shown by equation above. Here, ε_{ox} is the dielectric constant of the insulating layer and d_{ox} is the thickness of the insulating layer. These are independent of the applied voltage and the C_{ox} value does not change with the applied voltage. The change in the capacitance of the MIS structure is determined only by the Q_{sc} (space charge capacitance). Depending on the applied voltage, the states occurring in the MIS capacitance can be defined for a p-type semiconductor shown in Figure 2.9.

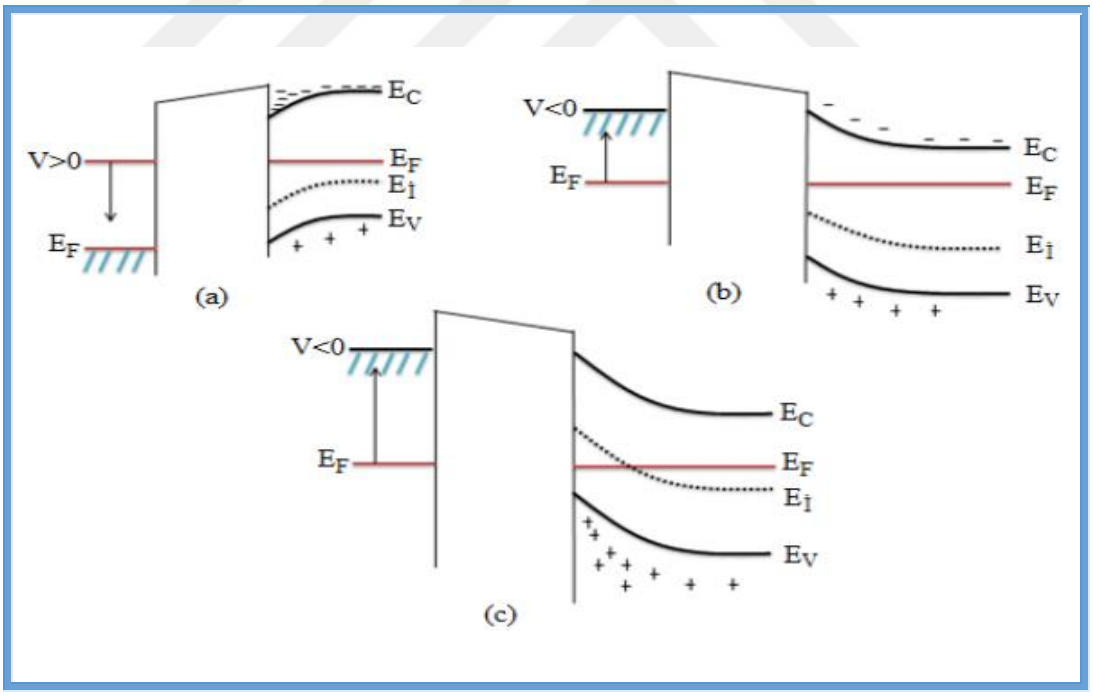

Figure 2.9. Energy band diagram of the ideal MIS structure at V≠0 (a) Accumulation (b) Depletion (c) Inversion [35]

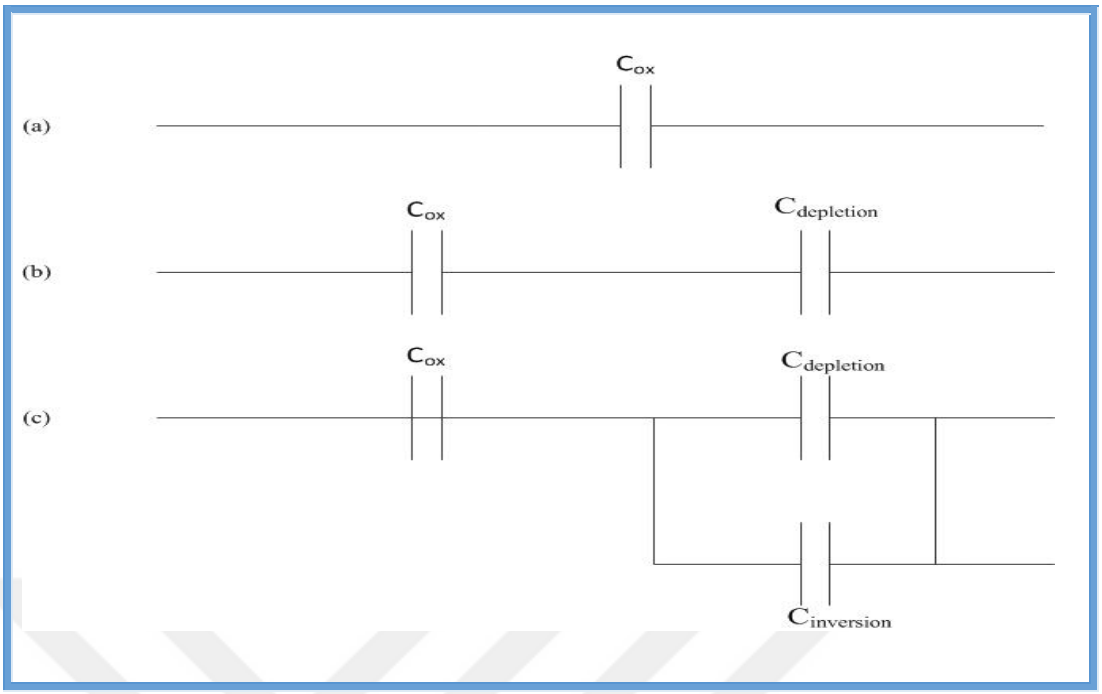

Figure 2.10. Electronic scheme of an ideal MIS structure in (a) Accumulation, (b) Depletion and (c) Inversion states [36].

2.3.2. Real MIS Structure

An ideal insulator has no space or moving charge in itself. In real structures, the insulating and semiconductor interface is never electrically neutral. The presence of trapped charges, called interface states in the insulator-semiconductor interface caused by impurities, and the presence of mobile ions, traps, constant oxide and interface charges, which occur depending on the method during oxidation, change the properties of the MIS structure. For these reasons, the ideal properties of the MIS structure have changed.

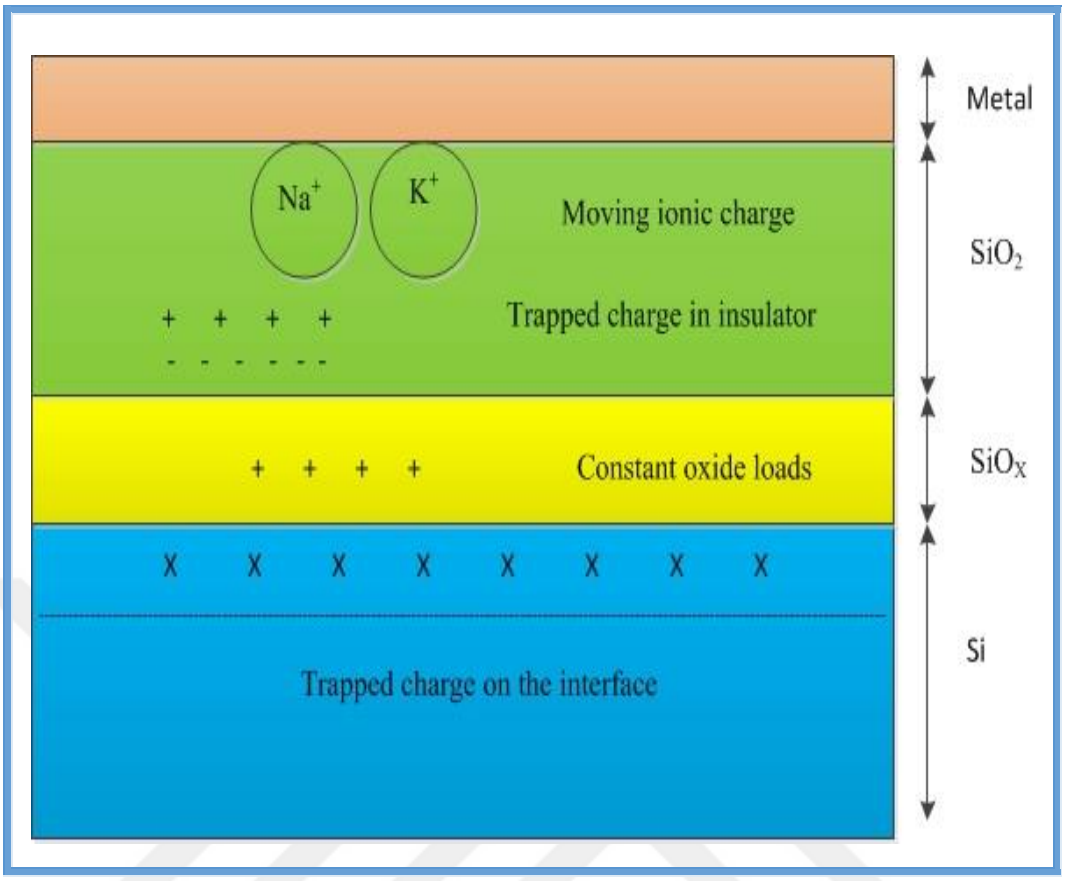

Figure 2.11. Interface states and classification of charges for a non-ideal MIS / MOS structure

These are respectively;

* Interface states defined in the insulator-semiconductor interface such as energy levels within the forbidden band gap,

* Fixed surface charges which immobile under the applied electric field and located on or near the semiconductor surface,

* Moving ions in the insulator,

* These are traps caused by exposure of the sample to radiation.

There are many situations and charges in a real MIS structure. The classification of these situations and charges is shown in Figure 2.11.

Interface state density theory in MIS structures

The presence of interface traps and insulating charges in an MIS structure will affect the ideal MIS characteristics. A foreign atom or a degradation in the crystal structure of a semiconductor leads to the emergence of energy levels in the forbidden energy zone. No matter how much the silicon surface is cleaned during an MIS construction, as a result of the irregularities in the crystal surface where the semiconductor braid is not removed, a large number of energy levels occur per unit area in the forbidden energy zone. These levels are called surface states [36].

Theoretical estimates for the density of surface states should be at the degree of density of the surface atoms, that is around 10^{15}cm^{-2}. Experimental results show that this is only in the degree of $\approx 10^{11} - 10^{13}\text{cm}^{-2}$ [36].

2.3.3. MFIS Structure

In recent years, there has been an increasing interest in ferroelectric memory elements. The reason for this is its applicability in new generation complex circuits. These circuit elements have potential advantages:

- Permanence
- unlimited write cycle
- low power consumption

Metal-ferroelectric-semiconductor structures have been the subject of technological studies as undamaged reading and high density memory devices. In Si and ferroelectric film interfaces, many problems are encountered, such as the formation of Si-based compounds, the presence of high density trap charges, the diffusion of elements into the Si semiconductor. However, preparing the ferroelectric / Si structure with good interface is quite difficult due to the diffusion of Si and ferroelectric material and chemical reactions. For this reason, MFIS structures are generally preferred. In order to solve these problems, the proposal to examine metal ferroelectric-semiconductor (MFIS) structures has emerged.

A schematic representation of an MFIS structure is given in Figure 2.12. These structures resemble a parallel plate capacitor, since one of the plates is metal and the other is semiconductor. Prominent features of this structure are determined by the

properties of the insulator and the insulator-semiconductor interface, as in the parallel plate capacitor.

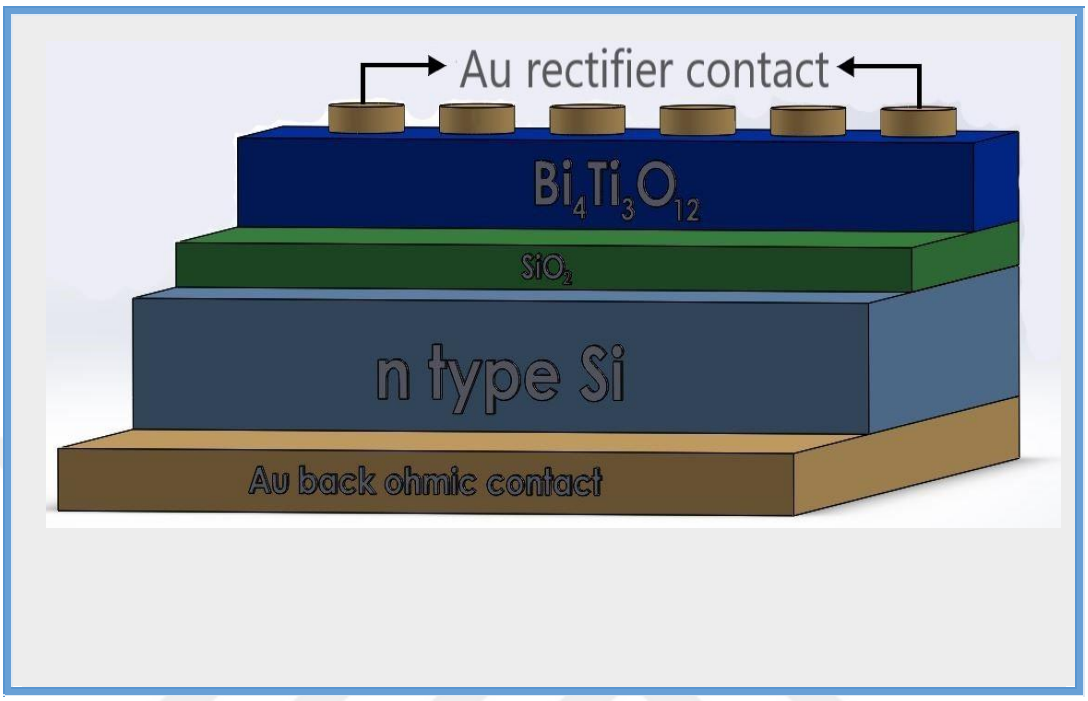

Figure 2.12. Schematic representation of the metal-ferroelectric-insulator-semiconductor structure

In this study, as ferroelectric material; $Bi_4Ti_3O_{12}$, as semiconductor material; oriented n-type Si with resistivity of 0.7 Ωcm (111) and as insulator SiO_2 was used. During the operation of the MFIS structure, considering the memory or excessive fatigue characteristics, it is thought to be promising structure and the most stable due to its reliability. It is easy to grow SiO_2 on silicon and creates a joint close to ideal mesh continuity. Therefore, reduces many surface effects and provides better control of joint characteristics. In BTO / Si interfaces, MFS structure has been transformed into MFIS structure by using a thin insulating layer such as Si_3N_4, SiO_2 and SnO_2. There are many methods of growing an insulating layer on the semiconductor. By thermal oxidation on Si, SiO_2 can be enlarged by passing dry O_2 at certain temperatures from the located at certain speeds. This process is most useful among many methods. This ultra-thin interface insulating layer (SiO_2) not only prevents internal diffusion between the ferroelectric film (BTO) and (Si) sample but also prevents the reduction of electric field in MFIS structures [3,10].

Insulating layer placed between ferroelectric material and semiconductor, not only isolate ferroelectric material and semiconductor from each other, but also regulate the charge transitions. In Figure 2.13, energy band diagrams of an MFIS structure are given for different working regions. When voltage is applied to the gate in an MFIS structure, it shows different results.

As seen in Figure 2.13 (a), when V_{GB}(applied gate voltage) = equal to V_{FB} (flatband voltage), the energy bands in the semiconductor are flat, not bent. In this case, there is no charge in the gate electrode of the semiconductor. As clearly seen from 2.13 (b), when $V_{GB} < V_{FB}$ (accumulation zone), positive charges accumulate on the surface of the semiconductor close to the oxide layer, the bending observed in the energy bands is observed in places close to the surface, and only the voltage in the oxide layer decreases.

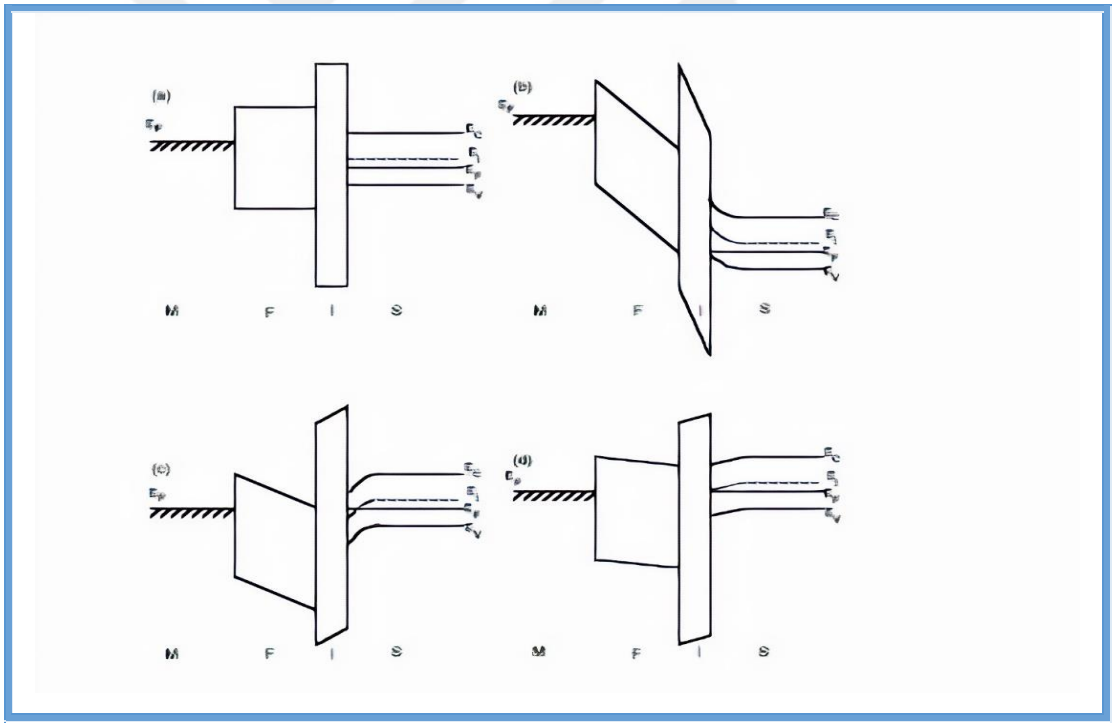

Figure 2.13. Energy band diagrams for different work zones for an MFIS structure

As seen in 2.13 (c) $V_{FB} < V_{GB} < V_{TH}$ (threshold) (depletion zone), due to space charges, a negatively charged field is created inside the semiconductor and this field increases with increasing voltage. As seen from 2.13 (d), when $V_{GB} > V_{TH}$ (inversion region), it

is seen that the conduction channel of the electrons is at the top level and the p-type semiconductor turns into the n-type.

From current-voltage measurements, the condition of the building in different regions can be obtained. To obtain a low frequency curve, while the structure is in equilibrium, capacitance is measured.

For the high frequency curve, low signal current, are performed measurements using a slow-changing, low-amplitude, high-frequency signal generator.

CHAPTER 3

EXPERIMENTAL METHOD

3.1. Experimental Preparation

Before starting the measurements, making the necessary experimental preparations, determining the measurement systems and steps to be used, provides more accurate measurement results. In this section, the creation steps of MFIS structure, physical and electrical characterization methods and measurement devices used are mentioned.

3.1.1. Creation of MFIS Structure

- $Bi_4Ti_3O_{12}$(BTO) thin films were deposited on the surface by spraying on (111) oriented and 0.7 Ω.cm resistivity n-Si semiconductor. Heated and compacted stoichiometric BTO powder is used.
- A mixture of Ar and O_2 gases was used as the working environment and the sample was kept at 700 ℃ for precipitation.
- This process allowed the formation of a thin layer of SiO_2 on the BTO / Si interface.
- A thin layer of SiO2 expands and grows at the BTO / Si interface during the annealing of BTO films in the air.
- The thickness of BTO thin films placed on the surface is approximately 2.4 μm. It was measured using the Veeco Dektak 6M thickness profilometer.
- The chemical composition of the films was determined using the local X-ray spectral method and scanning electron microscope (REM-101M). Here, spectral line densities of films are compared with the data of the sample determined as standard.

For electrical measurements, the top contacts (rectifier) have been created with the help of a mask, using pure Au (99.999%), approximately 2000 Å thick and 1 mm diameter circular points. Figure 3.1 (a) and (b) for the lower and upper contacts respectively the masks used are given. The upper contacts were formed on BTO films

by thermal evaporation method by using Leybold Univex 300 vacuum coating system in the Middle East Technical University Physics Department Solid State Laboratory.

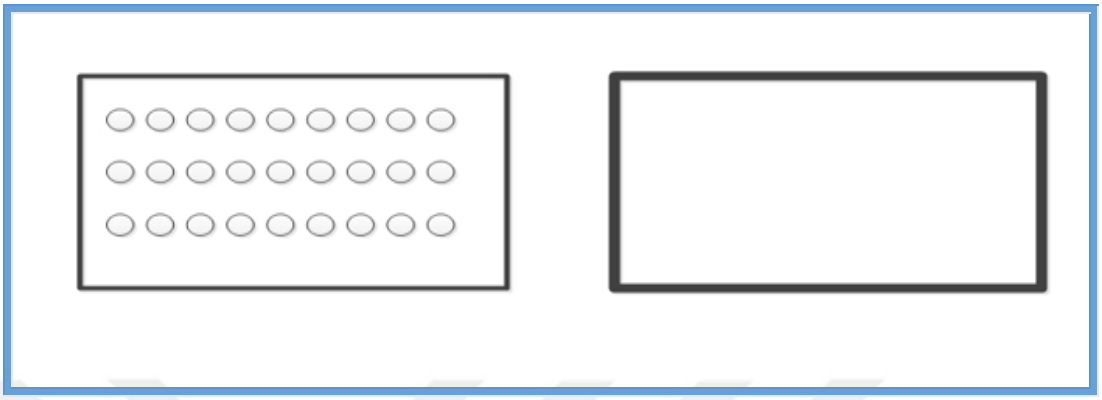

Figure 3.1. The schematic view of the copper masks used when forming the (a) top and (b) bottom contacts of the structure

The bottom contacts are also prepared on the back surface of the Si sample to form the MFIS structure and the structure is annealed at about 700 ℃ to form an ohmic contact. This was done in the Middle East Technical University Physics Department Solid State Laboratory. The mechanism used in Figure 3.2 is given [37].

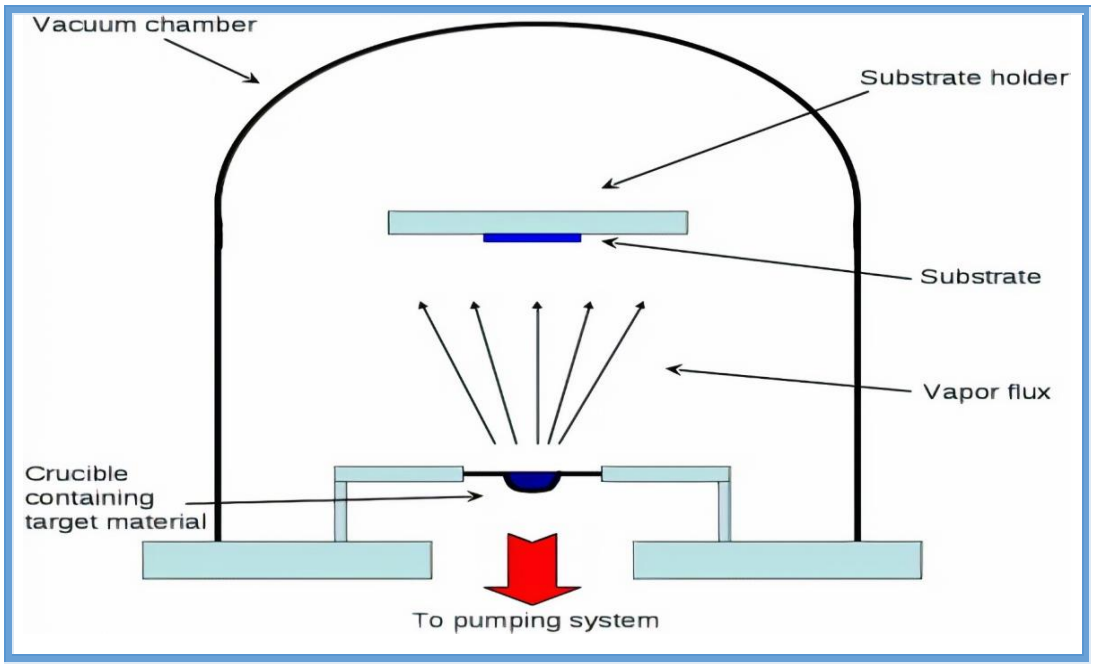

Figure 3.2. Vacuum device which used to create ohmic and rectifier contacts

A schematic diagram of the $Au/Bi_4Ti_3O_{12}/SiO_2/n\text{-}Si$ (MFIS) structure created in Figure 3.3 is given. Electrode connections for measurements were obtained using thin copper wires and conductive pure gold (Au).

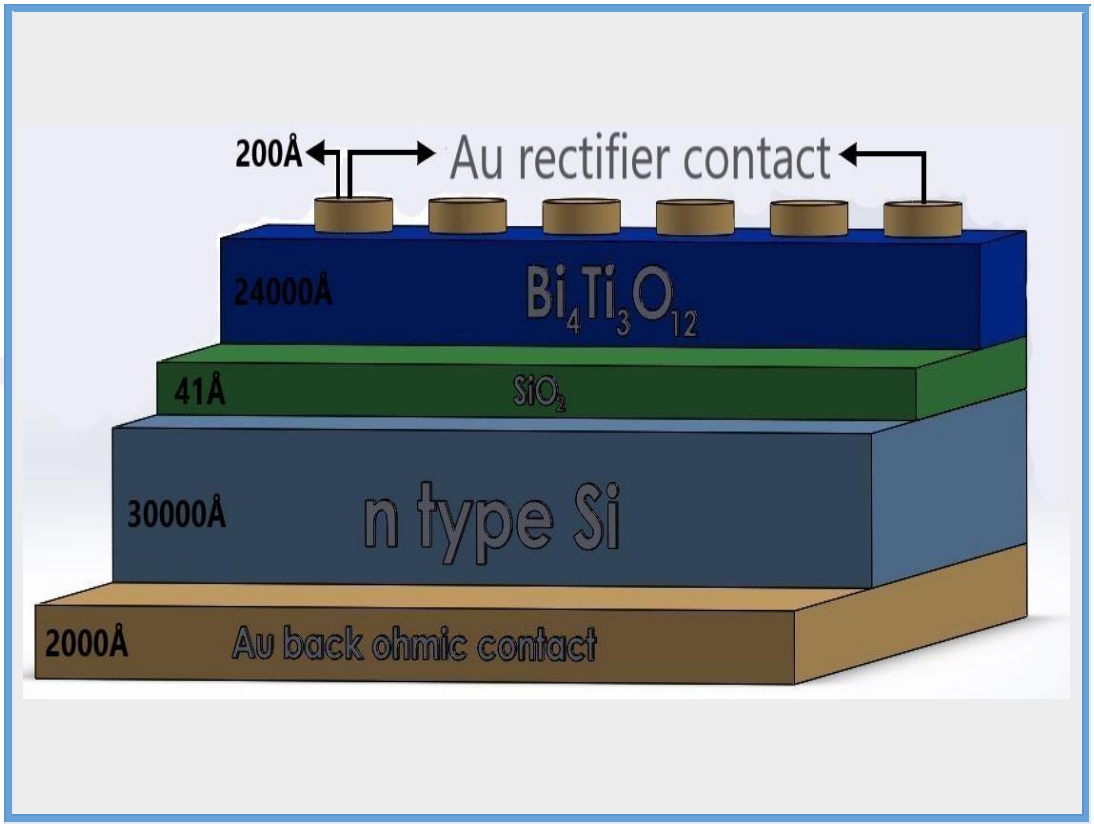

Figure 3.3. The cross-sectional areas of the created MFIS structure are shown schematically.

3.2. Experimental Measuring Devices

Sample was exposed to ^{60}Co γ-ray source at 5 kGy and 22 kGy, in nuclear research and training center Saraykoy which depends on Turkey Atomic Energy Agency. Schematic and photographic images of the experimental measurement system are given in Figure 3.4. and Figure 3.5., respectively.

1. Keithley 2400 current-voltage source
2. Janis vpf-475 cryostat

3.2.1. Keithley 2400 Current-Voltage Source

Keithley 2400 current-voltage source was used to measure current-voltage values with high accuracy. Keithley 2400 model current-voltage measuring device, which is shown in Figure 3.4, has the ability to measure both current voltage and voltage-based current. It can measure voltage from ± 1 μV to ± 200 V and current measurement from ± 10 pA to ± 1 A. The device, which can measure with high sensitivity like ± 0.15%, has IEEE-488 interface cables.



Figure 3.4. Keithley 2400 current-voltage source

3.2.2. Janis vpf-475 cryostat

I-V measurements of the Au/$Bi_4Ti_3O_{12}$/SiO_2/n-Si (MFIS) structure prepared were carried out in a Janis vpf-475 cryostat with 4 optical windows at a pressure of about 10^{-2} mbar. This cryostat which has Lake Shore model 321 temperature control system has the ability to measure between 79 K and 425 K temperature range.



Figure 3.5. Janis vpf-475 cryostat

CHAPTER 4

Results and Discussion

It is generally known that radiation has two important effects on materials that we can classify permanently and temporarily [27]. If deterioration occurs due to radiation effects in crystal lattices, which have great importance, permanent effects can be seen in the structures. Also, temporary effects may occur due to the generation of an electron-hole pair. To understand these effects in detail, the radiation impact on the I-V characteristics in MFIS structures has been investigated. I-V measurements were performed before radiation and after various radiation doses which consist of 5 kGy, 22 kGy. Forward and reverse-biases I-V data of the structure, before and after γ-ray irradiation from a ^{60}Co source, and measurements of which were carried out between -4/+6V, are presented in Fig. 4.1. I vs V plots of Au/$Bi_4Ti_3O_{12}$/SiO_2/n-Si (MFIS) structures have two distinct linear regions with different slopes as clearly seen from Fig. 4.1. The first linear region is expressed as Region I in the 0.12-0.38 V voltage range and the second linear region is expressed as Region II in the 0.40-0.80 V. Double Parallel Diode Model can be utilized to explain such multi-linear regions. As tabulated in Table 4.1, related with irradiation, three main parameters (Φ_{Bo}, I_o and n) of the structure for both Region I and Region II were acquired. Although the increase of the radiation dose to 22 kGy decreased the forward current value, it had no effect on the reverse bias current.

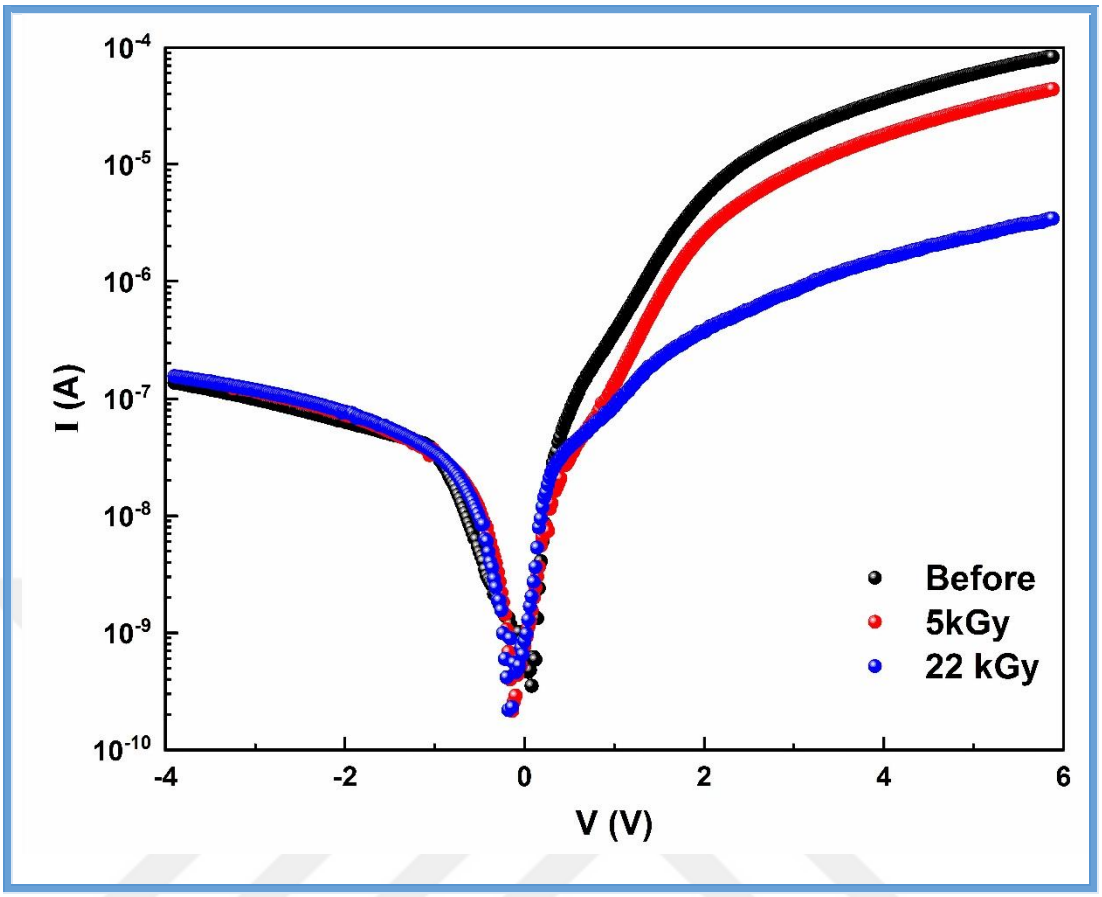

Figure 4.1. I-V graphs of the structure.

The correlation between current and applied forward biases can be written due to the thermionic emission (TE) as [38]

$$I = I_{o1}\left[\exp\left(\frac{q(V-IR_s)}{n_1 kT}\right)-1\right]+I_{o2}\left[\exp\left(\frac{q(V-IR_s)}{n_2 kT}\right)-1\right]+\frac{(V-IR_s)}{R_{sh}} \qquad \textbf{(4.1)}$$

In the formula, reverse saturation currents, Region I and Region II ideality factors and series and shunt resistors are shown with I_{o1} and I_{o2}, n_1 and n_2 and R_s and R_{sh}, respectively. Besides, IR_s corresponds to the voltage drop on the R_s Moreover, the components of diffusion and recombination generation currents were depicted by the first and second terms in Eq.4.1, respectively. Ln(I-V) plot's straight-lines interception was utilized for the extraction of I_{o1} and I_{o2} terms by the following expressions;

$$I_{o1} = AA^{*}T^{2}\exp\left(-\frac{q\Phi_{Bo1}}{kT}\right) \qquad I_{o2} = AA^{*}T^{2}\exp\left(-\frac{q\Phi_{Bo2}}{kT}\right) \qquad \textbf{(4.2)}$$

where the quantities A^{*} and A are the effective Richardson constant ($120 A/cm^2K^2$ for n-type Si) and the rectifier contact area (7.85×10^{-3} cm^2), respectively. Two linear regions slope at forward biases were utilized to determine the n values of MFIS structures as follows.

$$n_1 = \frac{q}{kT\tan\theta_1} \; n_2 = \frac{q}{kT\tan\theta_2} \qquad \textbf{(4.3)}$$

Thus, the value of Φ_{Bo} can be obtained from Eq.4.4 by using A and I_o,

$$\Phi_{Bo1} = \frac{kT}{q}\ln\left(\frac{AA^{*}T^{2}}{I_{o1}}\right) \; \Phi_{Bo2} = \frac{kT}{q}\ln\left(\frac{AA^{*}T^{2}}{I_{o2}}\right) \qquad \textbf{(4.4)}$$

In order to analyze radiation effects in more detail, it is of great importance to calculate some basic parameters such as n and Φ_{Bo}. Thus, the basic diode parameters calculated in the light of the equations given above are shown in Table 4.1.

Table 4.1. The basic electrical parameters of the structure.

	Region I			**Region II**		
	I_{o1} (A)	**n_1**	**Φ_{Bo1} (eV)**	**I_{o2} (A)**	**n_2**	**Φ_{Bo2} (eV)**
Before	2.15×10^{-10}	2.63	0.839	1.21×10^{-8}	10.89	0.738
5 kGy	1.14×10^{-9}	5.04	0.797	7.75×10^{-9}	14.25	0.749
22 kGy	2.25×10^{-9}	5.32	0.780	1.65×10^{-8}	23.73	0.730

	Ohm's Law	
	R_{sh} (Ω)	**R_s (Ω)**
Before	2.82×10^7	7.20×10^4
5 kGy	2.50×10^7	1.30×10^5
22 kGy	2.51×10^7	1.66×10^6

As clearly seen from Table (4.1.), I_o values increase after exposure of the structure to the with increasing radiation dose and it changed from 2.15×10^{-10} A to 2.25×10^{-9} A for Region I. I_o values for Region II changed from 1.21×10^{-8} A to 1.65×10^{-8} A. This radiation-induced change observed in I_o value could be attributed to the interfacial defect density increment [27]. There is an inverse proportion between the barrier height and reverse-saturation-current.

Depending on increasing irradiation dose, there was a decrease in Φ_{Bo} observed. According to some previous studies, γ-irradiation affects the free carrier concentration as it induces imperfections in the band gap at the junction of the semiconductor [35,36]. That's why radiation is an important factor for the barrier height in the structures and the barrier height value in the first region is close to the barrier height value in the second region and the value in the first region is higher than the value in the second region. According to recent studies in this field, X-ray photoelectron spectroscopy analysis points out defects generation which reduced the barrier height and enhanced tunneling effects, in Si dangling bonds [41].

While the values of ideality factor n in the first region were found to range from 2.63 at 0 kGy (before irradiation) to 5.32 at 22 kGy (after irradiation), values of ideality factor n in the first region were found to range from 10.89 at 0 kGy to 23.73 at 22 kGy. Obviously, the n values depend on the applied biases as first region values are much

lower than second region values. The barrier homogeneity and high N_{ss} density localized at the interlayer effects are seen as the cause of high values in Region II [10,37,38]. Other possible mechanisms that can lead to n values greater than unity can be listed as image force effect, recombination production, and tunneling [23,39].The ideality factor, which increases in parallel with the increase in applied radiation doses, is evidence of the deviation from the standard TE theory.

With the dose of radiation, defect and noise ratios occur that affect the performance of the structures. One of the important factors affecting this performance is resistance values. Utilizing from Ohm's law ($R_i = dV_i/dI_i$), the resistance (R_i) of the $Au/Bi_4Ti_3O_{12}/SiO_2/n\text{-}Si$ structure was calculated between -4V/6V. R_i values are extremely depending on biases as presented in Fig. 4.2. R_i values correspond to R_{sh} and R_s for high negative biases and high positive biases, respectively.

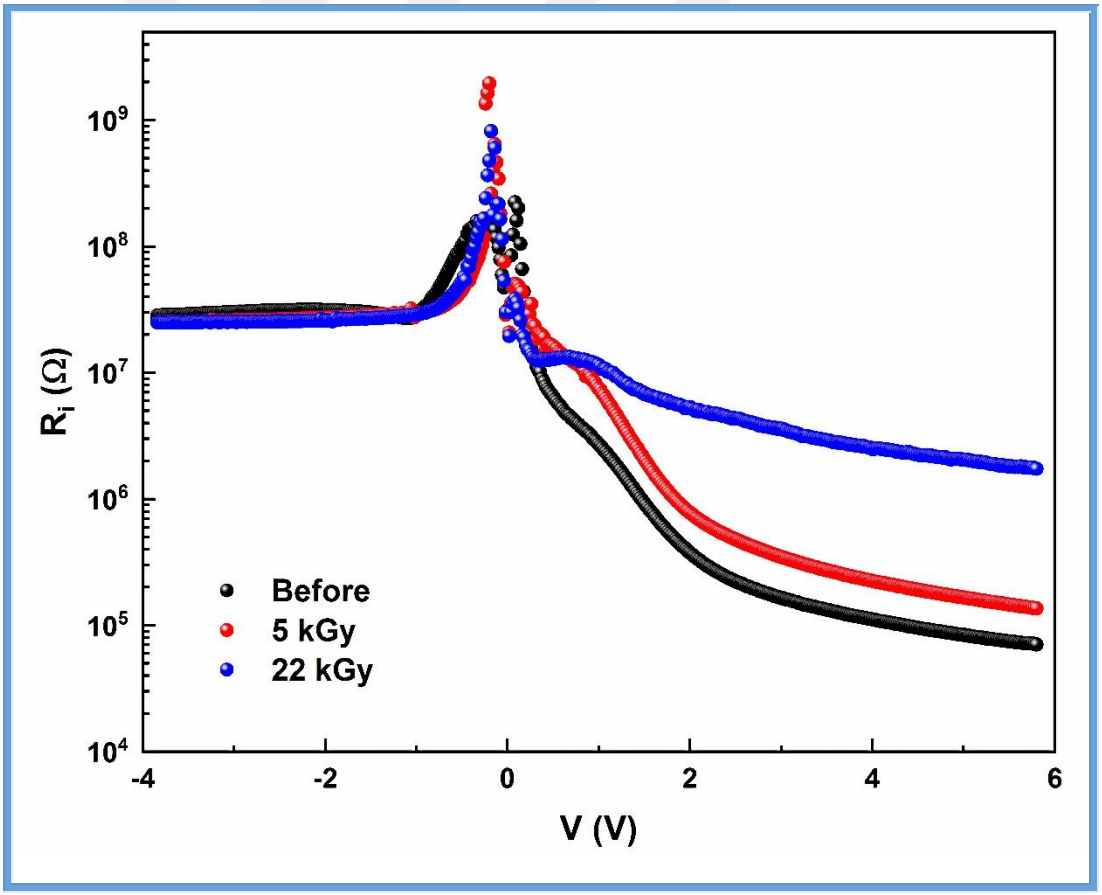

Figure 4.2. Ri characteristics of the structure.

According to Table (4.1), it was observed that R_{sh} values remained almost constant while R_s values increased in parallel with the increase in irradiation doses. This increase in R_s value indicates that free carrier density and mobility are reduced [44]. The reason for the decrease in mobility is the settlement of the defect centers that serve as a reunification center together with irradiation. The free carrier density will decrease when deep traps settle inside the material in relation to the displacement of the point defects. The intensity of irradiation-induced defect (trap) centers increases. Thus, the free carriers in the crystal lattice are captured by the defect (trap) centers, consequently, a decrease in the carrier density is observed.

Another way used to determine n, Φ_B, and R_s values is a method which carried out from the functions developed by Cheung method [45]. Cheung functions are defined using Eq (4.1) as follows:

$$\frac{dV}{dLn(I)} = n\frac{kT}{q} + R_s I \tag{4.5}$$

$$H(I) = V - n\frac{kT}{q}\ln\left(\frac{I}{AA^*T^2}\right) = n\Phi_{B(Cheung)} + R_s I \tag{4.6}$$

where Φ_{Bo} is the barrier height obtained from the intercept of H(I) vs I plots and IR_s is the voltage drop across the series resistance of MFIS structure. The dV/dLn(I) and H(I) -I curves obtained with the Cheung functions have linear lines and R_s values are obtained from the slope of these lines before and after the irradiation of the structure. Cheung functions curves for MFIS structure are given, in Fig. 4.6 for before radiation, Fig. 5 for 5 kGy and Fig. 6. for 22 kGy. All figures indicate that Cheung functions curves are linear lines. R_s, n and $\Phi_{B(Cheung)}$ values curves are given in Table 4.2. As can be seen in Table 4.2, the obtained R_s values by Cheung functions are compatible with each other and increase with the increasing irradiation. The values of $\Phi_{B(Cheung)}$ were found to decrease, while the values of *n* increase with the increasing radiation dose ($\Phi_{B(Cheung)}$ = 0.740 eV and *n* = 11.44 at 0 kGy and $\Phi_{B(Cheung)}$ = 0.705 eV and *n* = 26.80 at 22 kGy).

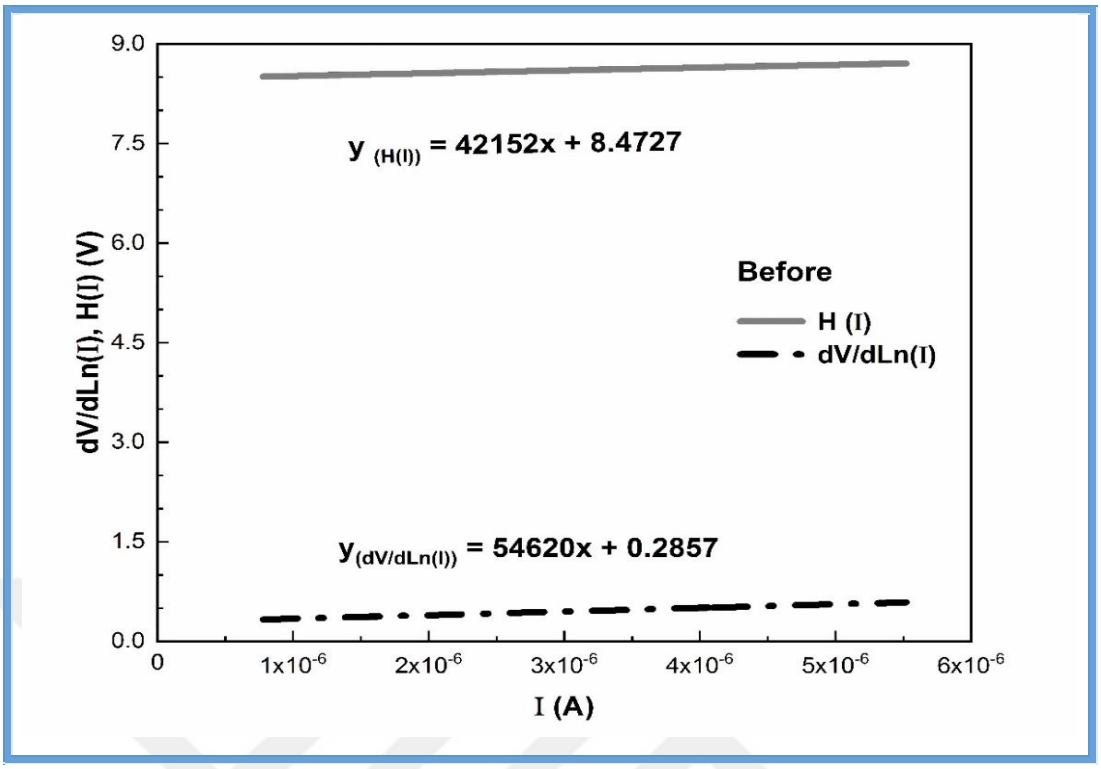

Figure 4.3. dV/d(LnI)/H(I)-I plots of the structure for before radiation.

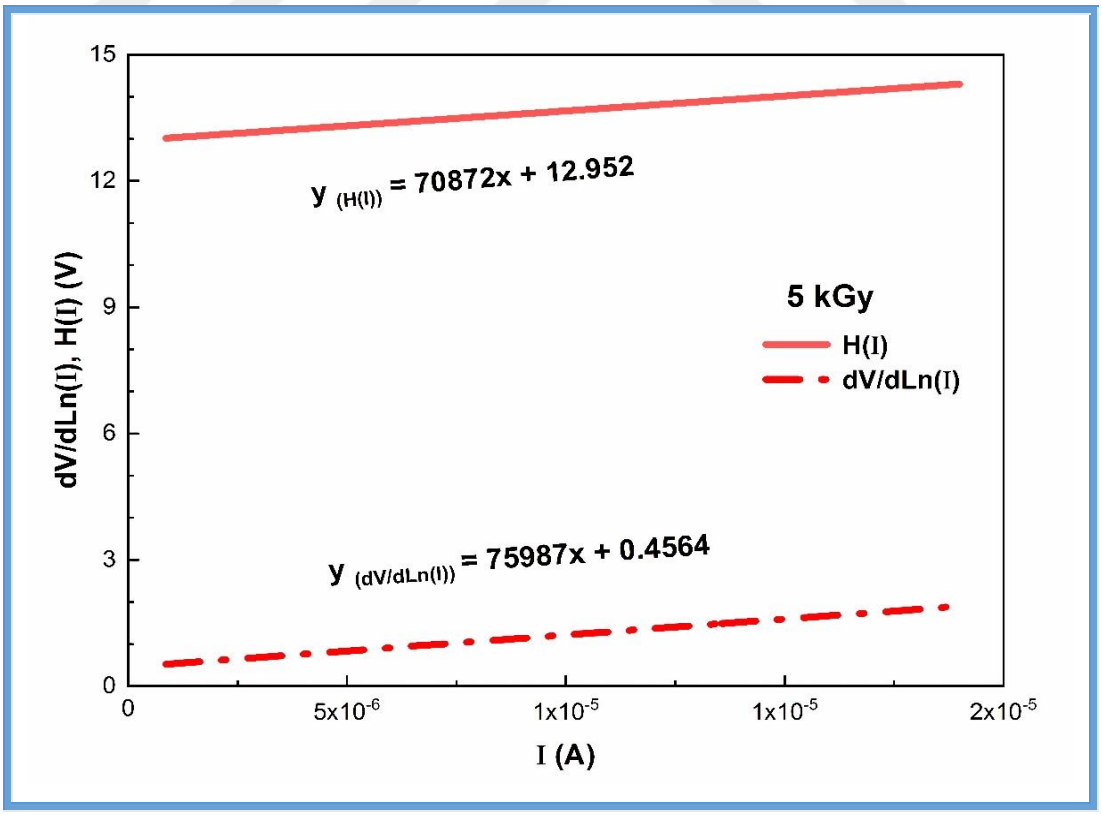

Figure 4.4. dV/d(LnI)/H(I)-I plots of the structure for 5 kGy.

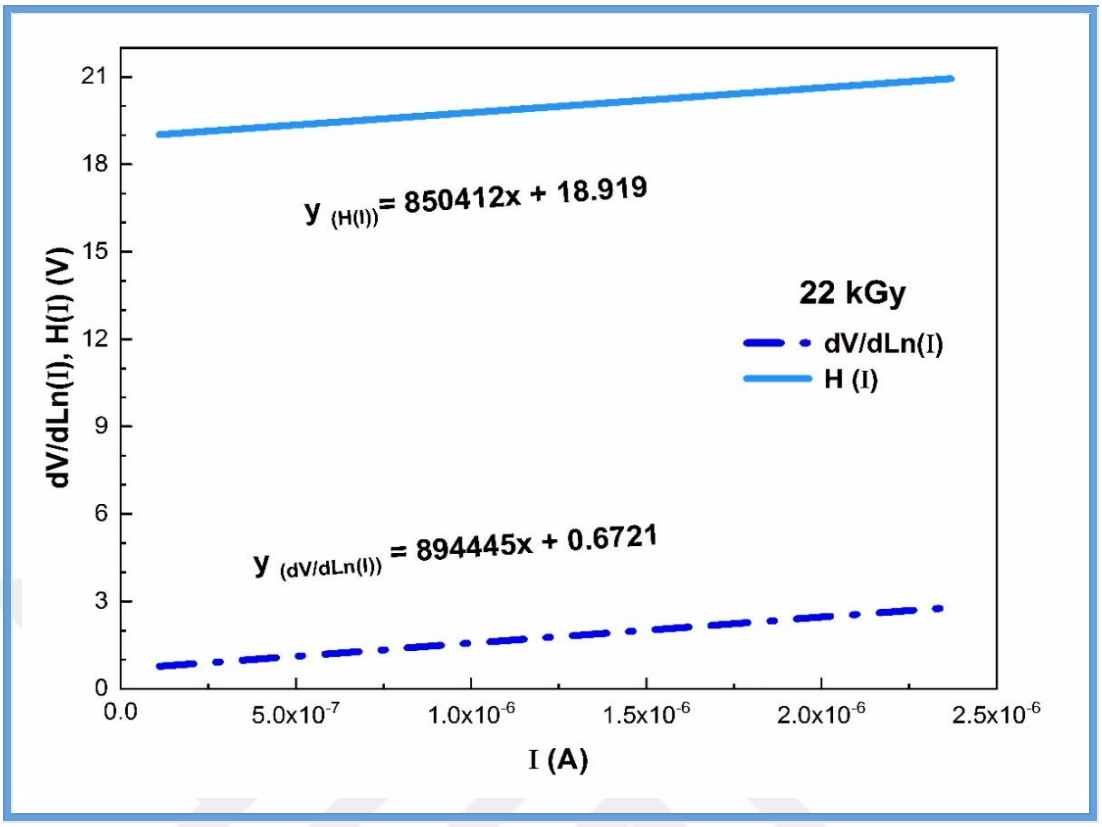

Figure 4.5. dV/dLn(I)/H(I)-I plots of the structure for 22 kGy.

Table 4.2. Basic electrical parameters of the structure obtained from Cheung Functions.

	dV/dLn(I) - I		**H(I) – I**	
	R_s (Ω)	**n**	**R_s (Ω)**	**$\Phi_{B(Cheung)}$ (eV)**
Before	5.46 x 10^4	11.44	4.22 x 10^4	0.740
5 kGy	7.60 x 10^4	18.00	7.09 x 10^4	0.722
22 kGy	8.94 x 10^5	26.80	8.50 x 10^5	0.705

On the other hand, as an alternative to the Cheung functions, another method can be also used presented by Norde to calculate some basic parameters [46]. Unlike Cheung functions, Norde function not only applied to the nonlinear region for the higher forward biases, but also applied to the full forward biases at I-V curve [47]. The modified Norde method is given as follows

$$F(V,\gamma)=\frac{V}{\gamma}-\frac{q}{kT}\ln\left(\frac{I}{AA^{*}T^{2}}\right) \tag{4.7}$$

where γ is the dimensionless value greater than the ideality factor which is extracted from the ln(I)-V plots. γ values are 16.34 at before radiation, 19.96 at 5 kGy and 30.85 at 22 kGy. Using the minimum point of F(V,γ) vs V plot, $F(V_o)$, $\Phi_{B(Norde)}$ and R_s can be obtained from the following equations, respectively.

$$\Phi_{B(Norde)}=F(V_o)+\frac{V_o}{\gamma}-\frac{kT}{q} \tag{4.8a}$$

$$R_s=\left(\frac{kT}{qI}\right)(\gamma-n) \tag{4.8b}$$

Fig. 4.7. shows the F(V) vs V plots for the $Au/Bi_4Ti_3O_{12}/SiO_2/n\text{-}Si$ (MFIS) structures. The values of Φ_{Bo} and R_s acquired from Eq. (4.8a) and (4.8b) under various irradiation conditions are presented in Table (4.2.). The values of R_s calculated from Norde and Cheung methods are different from each other. As clearly seen in Table (4.2.), the barrier height and series resistance (dV/dLn(I) vs I) values obtained from Norde theory is higher than the one extracted from Cheung's functions. These variations in values acquired by using different methods may be result from the extraction in change regions of the I-V curves. Furthermore, as we mentioned above, there are differences in the basic parameters as the areas of application of the Norde and Cheung are different from each other.

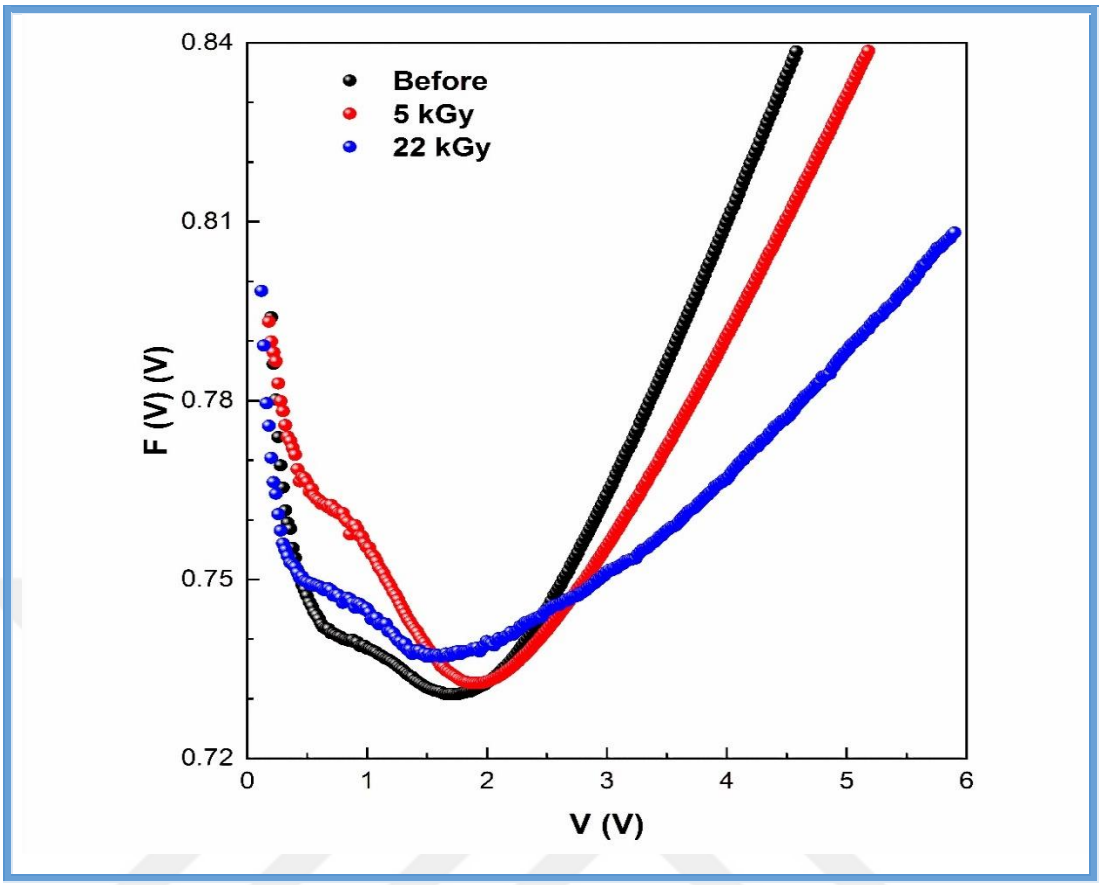

Figure 4.6. F(V)-V plots of the structure.

Table 4.3. Basic electrical parameters of the structure obtained from Norde Functions.

	Norde (Region I)		**Norde (Region II)**	
	R_s (Ω)	**$\Phi_{B(Norde)}$ (eV)**	**R_s (Ω)**	**$\Phi_{B(Norde)}$ (eV)**
Before	9.99×10^5	0.757	4.65×10^4	0.813
5 kGy	2.80×10^6	0.771	7.03×10^4	0.803
22 kGy	5.26×10^6	0.739	5.26×10^5	0.765

Considering the voltage-dependent n(V) and effective barrier height (Φ_e), N_{ss} in equilibrium with the semiconductor can be specified from the forward biases I-V data [48]. Regardless of R_s values, the values of Φ_e and n(V) can be calculated using Eq. (4.9) and Eq. (4.10). Φ_e is presumed to be voltage-dependent and derived by the following expression.

$$\Phi_e = \Phi_{B0} + \beta(V - IR_s) = \Phi_{B0} + \left(1 - \frac{1}{n(V)}\right)(V - IR_s) \quad \textbf{(4.9)}$$

Here, the voltage coefficient of the Φ_e is denoted by β. For MFIS structure having the N_{ss} in equilibrium with semiconductor and voltage-dependent ideality factor is expressed as,

$$n(V) = \frac{q}{kT}\left[\frac{(V - IR_s)}{\ln(I/I_0)}\right] = 1 + \frac{\delta}{\varepsilon_i}\left[\frac{\varepsilon_s}{W_D} + qN_{ss}(V)\right] \quad \textbf{(4.10)}$$

where the depletion layer width is denoted by W_D and the interlayer and semiconductor permittivities are denoted by ε_i and ε_s, respectively. This expression of n(V) is identical to Eq. (4.11) of Card and Rhoderick [49] and the expression for N_{ss} is converted to

$$N_{ss}(V) = \frac{1}{q}\left[\frac{\varepsilon_i}{\delta}(n(V) - 1) - \frac{\varepsilon_s}{W_D}\right] \quad \textbf{(4.11)}$$

where δ, the interlayer thickness (SiO_2) was obtained from the C-V measured at 1 MHz in the strong accumulation region by using the $C_{ox} = \varepsilon_i\varepsilon_o A/\delta$ and found to be 41 Å in the previous study. Then again, the interface states energy, E_{ss}, to the conduction band's bottom, E_c, at the semiconductor's surface is derived by [50]

$$E_c - E_{ss} = q(\Phi_e - V) \quad \textbf{(4.12)}$$

the energy distribution profile of N_{ss} as a function of ($E_c - E_{ss}$) were obtained from the forward bias I-V characteristics by taking the bias dependence of the Φ_e into account for each radiation dose. As seen in Fig. 8, the exponential growth of the N_{ss} from the with the semiconductor mid-gap toward the bottom of the conduction band is very apparent. The N_{ss} values extracted without considering the R_s are higher than those

obtained taking into account the R_s. In addition, these decreases of interface states with increasing irradiation doses were attributed to the recombination of electron-hole pairs under the radiation and the existence of an interlayer (SiO_2) at MFIS interface. Hence, R_s must be considered in calculations of basic electrical parameters.

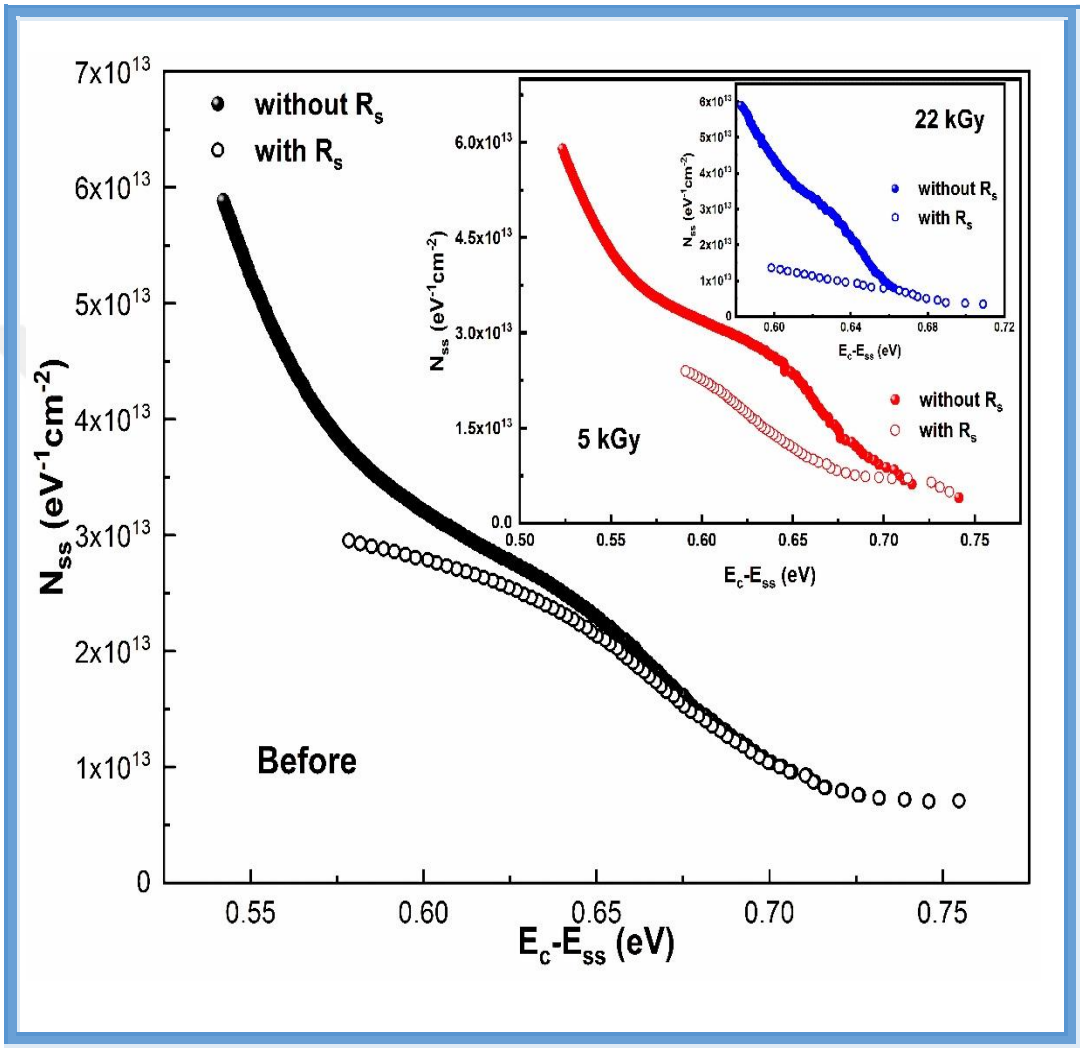

Figure 4.7. The density of N_{ss} profiles as a function of (E_c-E_{ss}).

CHAPTER 5

CONCLUSION

Investigation of electrical properties of metal-ferroelectric-insulator-semiconductor structures at certain radiation doses gives us very important information about current-voltage characteristics of these structures. In recent years, there are many experimental results in the literature on MFIS structures. However, in the studies carried out on these structures, the thickness of the insulating layer grown between the metal and the semiconductor, the series resistance of the structure, and the effects of the interface conditions on I-V are still not clarified. Studies on the inhomogeneity of the insulating layer, the formation of the potential barrier between the metal and the semiconductor, and the transmission mechanisms of the interface states are ongoing.

In this thesis, firstly, structural analysis of $Bi_4Ti_3O_{12}$ thin film was performed. In order to determine the surface morphology of the BTO film, certain methods were used and an image of the surface morphology was obtained. The sample surface gives a very smooth and dense appearance. No remarkable flaws and cracks appear. The hysteresis curve of the structure at different radiation doses has been obtained and it has been determined that it shows ferroelectric properties.

The forward and reverse biases I-V characteristics of $Au/Bi_4Ti_3O_{12}/SiO_2/n\text{-}Si$ (MFIS) structures which exposed to ^{60}Co γ-irradiation of doses ranging from 0 to 22 kGy have been investigated at room temperature. While the forward current was detected to decrease with radiation dose increment; the irradiation effects on the reverse bias current were almost negligible. According to the experimental results, it was observed that the main electrical parameters such as I_o, n, Φ_B, R_s and R_{sh} values were strongly dependent on the irradiation effect. Among main parameters which exposure to increasing cumulative γ-ray doses, while the values of the ideality factor have an apparent increase, the values of zero-bias barrier height have a decrease. Growth in n values which increase with irradiation dose result from inhomogeneity of the interlayer and the presence of a thin insulating layer. On the other hand, another important parameter, R_s was obtained by three different methods: Ohm's Law, Cheung and

Norde methods. Also, results obtained from these methods showed greatly compatibility with each other. The density of interface states (N_{ss}) which was determined from the forward bias I-V characteristics by considering the bias dependence of the Φ_e and n, decreases with radiation dose increment. Such a behavior of N_{ss} was attributed to the decrease in the recombination centers and because of the irradiation and reordering/restructuring of the band-gap surface states. In conclusion, the irradiation-dependent I-V characteristics affirmed that, R_s and N_{ss} are significant parameters that considerably affect the electrical qualifications of MFIS structures.

As a result of the exposure of the structure to the gamma-ray source with increasing doses, an increase in the forward saturation currents was observed in parallel with the increase in the doses. It has been determined that the ideality factor is considerably larger than 1 irrespective of radiation. Obtained before irradiation and after all radiation dose levels, the high n values indicated are indications of deviation from the standard TE theory. According to the results obtained, n values in the second region are higher than n values in the first region. And with increasing radiation dose, n values in both regions also increased. Gamma-irradiation can cause some defects in the band gap at the junction of the semiconductor. These defects can also affect the free carrier concentration, leading to a decrease or increase in the barrier height of the materials. The Φ_{B0} values in this material tended to decrease due to increasing irradiation doses, resulting in an almost regular increase of forward bias currents. A reduction in the height of the barrier due to radiation is known more in the literature as the Poole-Frenkel effect, which is attributed to the thermal production of carriers. R_s values increase with increasing radiation doses. In N_{ss} profiles obtained depending on the radiation doses, it was observed that the interface states decreased exponentially from the mid-band gap of the semiconductor to the upper edge of the valence band. In addition, decreases in N_{ss} values with increased irradiation doses are attributed to the recombination of electron-hall pairs under radiation. In addition, it has been attributed to the reorganization and reconstruction of the band-space interface states under the electric field.

As a result, it was observed that no significant defect or deterioration occurred in the applied dose range that would prevent the operation of this MFIS type structure. This

result is a very important observation for radiation resistant production of materials such as solar cells, diodes, capacitors and transistors. The production of radiation-resistant electronic materials for use in the space environment is very important in terms of increasing the operational reliability of satellite systems. On the other hand, some devices used in biomedical and industrial applications may be exposed to similar radiation effects, and the safe operation of these devices depends on the production of radiation-resistant materials. In other words, production of radiation-resistant electronic materials is needed, especially in space, nuclear industry and biomedical applications. In this context, it is thought that this thesis study will be interesting and will make important contributions to the literature.

FUTURE WORK

Some suggestions that may be a continuation of this study and thus increase the scope of the study are as follows:

- In order to better evaluate the effect and radiation-related results of the interface layer thickness, materials with different layers of intermediate layers can be produced and compared under the same radiation doses.
- Calculations can be extended by performing I-V measurements at high and low frequencies before and after each irradiation dose.
- Especially, radiation doses in the range of 5-22 kGy can be tightened or higher doses can be observed and the behavior of the same material at higher doses can be observed.
- It can be observed at which level that the radiation effects change depending on the time by taking measurements at certain intervals after each radiation dose or after the highest irradiation dose.
- In addition to the change in radiation doses, measurements depending on temperature and light can also be taken so that the effect of temperature on irradiated samples can be evaluated.

REFERENCES

[1] D. Wijethunge, C. Tang, C. Zhang, L. Zhang, X. Mao, and A. Du, 'Bandstructure engineering in 2D materials using Ferroelectric materials', *Appl. Surf. Sci.*, vol. 513, no. December 2019, p. 145817, 2020.

[2] X. Liu, K. Zhao, and Y. Yang, 'Effective polarization of ferroelectric materials by using a triboelectric nanogenerator to scavenge wind energy', *Nano Energy*, vol. 53, pp. 622–629, 2018.

[3] C. Liu, J. Wang, G. Xu, M. Kamlah, and T. Y. Zhang, 'An isogeometric approach to flexoelectric effect in ferroelectric materials', *Int. J. Solids Struct.*, vol. 162, pp. 198–210, 2019.

[4] G. R. Fox, F. Chu, and T. Davenport, 'Current and future ferroelectric nonvolatile memory technology', *J. Vac. Sci. Technol. B Microelectron. Nanom. Struct.*, vol. 19, no. 5, pp. 1967–1971, 2001.

[5] S. K. Badge and A. V. Deshpande, 'Effect of vanadium doping on structural, dielectric and ferroelectric properties of bismuth titanate ($Bi_4Ti_3O_{12}$) ceramics', *Ceram. Int.*, vol. 45, no. 12, pp. 15307–15313, 2019.

[6] W. Gao, Y. Zhu, Y. Wang, G. Yuan, and J. M. Liu, 'A review of flexible perovskite oxide ferroelectric films and their application', *J. Mater.*, vol. 6, no. 1, pp. 1–16, 2020.

[7] Nishi, Y. (Ed.). Advances in Non-volatile Memory and Storage Technology (2th. ed.). Sawston, MA: Woodhead Publishing 2019

[8] B. Zeng *et al.*, 'Program/Erase Cycling Degradation Mechanism of HfO2-Based FeFET Memory Devices', *IEEE Electron Device Lett.*, vol. 40, no. 5, pp. 710–713, 2019.

[9] M. Fitsilis, 'Scaling of the Ferroelectric Field Effect Transistor and Programming Concepts for Non-volatile Memory Applications', *Simulation*,

2005.

[10] C. Long, H. Fan, W. Ren, and J. Zhao, ‘Double polarization hysteresis and dramatic influence of small compositional variations on the electrical properties in Bi4Ti3O12 ceramics’, *J. Eur. Ceram. Soc.*, vol. 39, no. 14, pp. 4103–4112, 2019.

[11] P. Durmus and S. Altindal, ‘Two-diode behavior in metal-ferroelectric-semiconductor structures with bismuth titanate interfacial layer’, *Int. J. Mod. Phys. B*, vol. 31, no. 27, 2017.

[12] S. K. Badge and A. V. Deshpande, ‘Study of dielectric and ferroelectric properties of Bismuth Titanate ($Bi_4Ti_3O_{12}$) ceramic prepared by sol-gel synthesis and solid state reaction method with varying sintering temperature’, *Solid State Ionics*, vol. 334, no. July 2018, pp. 21–28, 2019.

[13] Z. S. Macedo, M. H. Lente, J. A. Eiras, and A. C. Hernandes, ‘Dielectric and ferroelectric properties of Bi4Ti 3O12 ceramics produced by a laser sintering method’, *J. Phys. Condens. Matter*, vol. 16, no. 16, pp. 2811–2818, 2004.

[14] P. Durmuş, M. Yildirim, and Ş. Altindal, ‘Controlling the electrical characteristics of Al/p-Si structures through Bi4Ti3O12 interfacial layer’, *Curr. Appl. Phys.*, vol. 13, no. 8, pp. 1630–1636, 2013.

[15] H. Search, C. Journals, A. Contact, and M. Iopscience, ‘Analyses of High Frequency Capacitance – Voltage Characteristics of Metal-Ferroelectrics-Insulator-Silicon Structure Analyses of High Frequency Capacitance – Voltage Characteristics of Metal-Ferroelectrics-Insulator-Silicon Structure’, vol. 2044.

[16] G. Pahwa, T. Dutta, A. Agarwal, and Y. S. Chauhan, ‘Compact model for ferroelectric negative capacitance transistor with MFIS structure’, *IEEE Trans. Electron Devices*, vol. 64, no. 3, pp. 1366–1374, 2017.

[17] C. K. Lee, W. S. Kim, H. H. Park, H. Jeon, and Y. H. Pae, ‘Thermal-stress stability of yttrium oxide as a buffer layer of metal-ferroelectric-insulator-semiconductor field effect transistor’, *Thin Solid Films*, vol. 473, no. 2, pp. 335–

339, 2005.

[18] I. Taşçioğlu, A. Tataroğlu, A. Özbay, and Ş. Altindal, ‘The role of 60Co γ-ray irradiation on the interface states and series resistance in MIS structures’, *Radiat. Phys. Chem.*, vol. 79, no. 4, pp. 457–461, 2010.

[19] A. Kahraman and E. Yilmaz, ‘Irradiation response of radio-frequency sputtered Al/Gd2O3/p-Si MOS capacitors’, *Radiat. Phys. Chem.*, vol. 139, no. December 2016, pp. 114–119, 2017.

[20] R. Medwal, S. Gupta, S. P. Pavunny, R. K. Katiyar, R. Thomas, and R. S. Katiyar, ‘Low-voltage-driven Pt/BiFeO3/DyScO3/p-Si-based metal–ferroelectric–insulator–semiconductor device for non-volatile memory’, *J. Mater. Sci.*, vol. 53, no. 6, pp. 4274–4282, 2018.

[21] W. B. Wilson and A. D. Campiglia, ‘Determination of polycyclic aromatic hydrocarbons with molecular weight 302 in water samples by solid-phase nano-extraction and laser excited time-resolved shpol’skii spectroscopy’, *Analyst*, vol. 136, no. 16, pp. 3366–3374, 2011.

[22] M. J. Stowell, ‘Metals and materials; science, processes, applications’, *Int. Mater. Rev.*, vol. 40, no. 5, pp. 218–218, 1995.

[23] Altındal, S., “ Al - SiOx - pSi aygıtların ve günes pillerinin elektriksel karakteristikleri.”, Doktora Tezi, Gazi Üniversitesi Fen Bilimleri Enstitüsü,Ankara, 52-74 (1993).

[24] D. G. Popescu, M. A. Husanu, C. Chirila, L. Pintilie, and C. M. Teodorescu, ‘The interplay of work function and polarization state at the Schottky barriers height for Cu/BaTiO3 interface’, *Appl. Surf. Sci.*, vol. 502, no. December 2018, p. 144101, 2020.

[25] Moll J.L., Tarui Y., “A new solid state memory resistor”, IEEE Trans. Electron Devices, ED-10, 338-341 (1963).

[26] M. Yıldırım, C. Şahin, Altındal, and P. Durmuş, ‘Electrical and Dielectric

Properties of a n-Si Schottky Barrier Diode with Bismuth Titanate Interlayer: Effect of Temperature', *J. Electron. Mater.*, vol. 46, no. 3, pp. 1895–1901, 2017.

[27] Ö. Güllü, M. Çankaya, M. Biber, and A. Türüt, 'Gamma irradiation-induced changes at the electrical characteristics of organic-based Schottky structures', *J. Phys. D. Appl. Phys.*, vol. 41, no. 13, 2008.

[28] A. Tataroğlu and Ş. Altindal, 'Gamma-ray irradiation effects on the interface states of MIS structures', *Sensors Actuators, A Phys.*, vol. 151, no. 2, pp. 168–172, 2009.

[29] Winokur, P. S., Schwank, J. R., McWhorter, P. J., Turpin, D. C., and Dressendorfer, P. V., "Correlating the Radiation Response of MOS Capacitors and Transistors", IEEE Transactions On Nuclear Science, 31 (6): 1453–1460 (1984).

[30] E. F. da Silva Jr., Y. Nishioka, and T.-P. Ma, IEEE Trans. Nucl. Sci. NS-34,

1190 (1987).

[31] B. R. Hahn and D. Y. Yoon, 'Electrical and interfacial properties of metal-polyimide-silicon structures', *J. Appl. Phys.*, vol. 65, no. 7, pp. 2766–2771, 1989.

[32] Terman L. M., "An investigation of surface states at a silicon-silicon dioxide interface employing metal-oxide-silicon diodes", Solid-State Electronics, 5(5): 259-285 (1962).

[33] Leistiko, O., Grove, A. S., and Sah, C. T., "Electron and hole mobilities in inversion layers on thermally oxidized silicon surfaces." IEEE Trans. Electron Devices ED-12, pp. 248-254, 1965.

[34] Sharma B.L., "Metal-Semiconductor Contacts Schottky Barrier Junctions and Their Applications", 1st ed., Plenum Press, New York, 113-118 (1984).

[35] R. K. Jha, P. Singh, M. Goswami, and B. R. Singh, 'Impact of plasma enhanced

atomic layer deposited HfO2 buffer layer on the structural, electrical and ferroelectric properties of metal/ferroelectric/insulator/semiconductor gate stack for non-volatile memory applications', *J. Mater. Sci. Mater. Electron.*, vol. 30, no. 16, pp. 15224–15235, 2019, doi: 10.1007/s10854-019-01895-9.

[36] Cooke M. J., "Semiconductor Devices", Prentice Hall, New York, 294-308 (1990).

[37] S. Nezhadesm-Kohardafchahi, S. Farjami-Shayesteh, Y. Badali, Altındal, M. A. Jamshidi-Ghozlu, and Y. Azizian-Kalandaragh, 'Formation of ZnO nanopowders by the simple ultrasound-assisted method: Exploring the dielectric and electric properties of the Au/(ZnO-PVA)/n-Si structure', *Mater. Sci. Semicond. Process.*, vol. 86, no. June, pp. 173–180, 2018.

[38] H. U. Tecimer, M. A. Alper, H. Tecimer, S. O. Tan, and Altındal, 'Integration of Zn-doped organic polymer nanocomposites between metal semiconductor structure to reveal the electrical qualifications of the diodes', *Polym. Bull.*, vol. 75, no. 9, pp. 4257–4271, 2018.

[39] S. J. Fonash, S. Ashok, R. Singh, S. J. Fonash, S. Ashok, and R. Singh, 'Effect of ion-beam sputter damage on Schottky barrier formation in silicon Effect of ion-beam sputter damage on Schottky barrier formation in silicon', vol. 423, no. 1981, pp. 1–4, 2006.

[40] E. Grusell, S. Berg, and L. P. Andersson, J. Electrochem. Soc. 127, 1573–1576 (1980).

[41] Y. Xu, J. Bi, K. Xi, and M. Liu, 'The effects of γ-ray irradiation on graphene/n-Si Schottky diodes', *Appl. Phys. Express*, vol. 12, no. 6, 2019.

[42] S. O. Tan, H. Tecimer, and O. Çiçek, 'Comparative Investigation on the Effects of Organic and Inorganic Interlayers in Au / n-GaAs Schottky Diodes', vol. XX, no. Xx, pp. 1–7, 2017.

[43] M. M. Bülbül and S. Zeyrek, 'Frequency dependent capacitance and conductance-voltage characteristics of Al/Si3N4/p-Si(1 0 0) MIS diodes',

Microelectron. Eng., vol. 83, no. 11–12, pp. 2522–2526, 2006.

[44] A. Teffahi *et al.*, 'Effect of 60Co γ-ray irradiation on electrical properties of Ti/Au/GaAs1-xNx Schottky diodes', *Curr. Appl. Phys.*, vol. 16, no. 8, pp. 850–858, 2016.

[45] S. K. C. W. Cheung, 'Extraction of Schottky diode parameters from forward current-voltage characteristics Extraction of Schottky diode parameters from forward current-voltage characteristics', vol. 85, no. 1986, 2014.

[46] Sze S. M., "Physics of Semiconductor Devices", 2nd ed., John Wiley & Sons, New York, 362-390 (1981).

[47] M. Emin Fırat, M. Akif Taştan, and Ş. Karataş, 'Comparison of electrical characteristics of Sn/p-type Si structure at different temperatures and under irradiation', *Mater. Today Proc.*, vol. 18, pp. 1946–1954, 2019.

[48] S. Demirezen, Z. Sönmez, U. Aydemir, and S. Altındal, 'Effect of series resistance and interface states on the I-V, C-V and G/ω-V characteristics in Au/Bi-doped polyvinyl alcohol (PVA)/n-Si Schottky barrier diodes at room temperature', *Curr. Appl. Phys.*, vol. 12, no. 1, pp. 266–272, 2012.

[49] H. Search, C. Journals, A. Contact, M. Iopscience, and I. P. Address, 'Studies of tunnel MOS diodes I . Interface effects in silicon Schottky diodes', vol. 1589, 1971.

[50] H. Uslu, Ş. Altindal, U. Aydemir, I. Dökme, and I. M. Afandiyeva, 'The interface states and series resistance effects on the forward and reverse bias I-V, C-V and G/ω-V characteristics of Al-TiW-Pd 2Si/n-Si Schottky barrier diodes', *J. Alloys Compd.*, vol. 503, no. 1, pp. 96–102, 2010.

CURRICULUM VITAE

PERSONAL INFORMATION

Surname, Name	DULKADİR,SEZGİN
Date of Birth	26/09/1993
Place of Birth	KIRIKKALE/TURKEY
Nationality	Turkish (T.C)
Phone	05067181472
Home address	Güzeltepe Mah. 551. Sok 8/18 Hakan İnş. Kırıkkale/Merkez

EDUCATION

2017 - 2020	M.Sc Ankara Yıldırım Beyazıt University, Electrical and Electronics Engineering, Ankara/TURKEY
2012-2017	B.Sc Ankara Yıldırım Beyazıt University, Electrical and Electronics Engineering,

Ankara/TURKEY

2008-2012 Osmangazi Fen Lisesi

Kırıkkale/TURKEY

WORK EXPERIENCE

July 2019 - Research Assistant

Karabuk University

Summer 2016 Intern, VESTEL SAVUNMA
Ankara, TURKEY

Summer 2016 Intern, ASELSAN
Ankara, TURKEY